Faculty of Science and Technology

MASTER'S THESIS

Study program / Specialization: Petroleum technology	Spring semester, 2013 Open
Writer: Kim I.M. Flatråker	…… (Writer's Signature)
Faculty Supervisor: Rune W. Time Supervisors: Rune W. Time, Hermonja A. Rabenjafimanantsoa ("Benja").	
Title of thesis: Hydrodynamic Oscillations of Non-Newtonian fluids in a U-tube.	
Credits (ECTS) : 30	
Key words • Oscillation • Rheology • Viscoelasticity • Numerical Simulator • Polymer CMC	Pages: 48 + Appendix Stavanger, 14/6 – 2013 (Date / Month – Year)

ACKNOWLEDGEMENTS

I would like to raise my sincere gratitude towards my supervisors Professor Rune Time and Senior Engineer Benja. Benja has been available every single day throughout my time in the lab. His great enthusiasm for his work is highly contagious and he has been a huge motivator for me. Professor Rune Time is a very knowledgeable person, and has been a tremendous help while writing my thesis. Rune was also generous enough as to help me with all the Matlab simulators.
Thank you both for your time and dedication.
I am also grateful to Bachelor Students Ingeborg Elin Kvamme and Kristine Høyland Tjelta for their participation in the rheological measurements.

Kim Flatråker

ABSTRACT

In this thesis, a five meter high flow rig has been constructed in the form of a U-tube. Several experiments were conducted in order to investigate rheological parameters in an oscillating flow with the intention of gaining knowledge of how these parameters are transferred from a small scale lab test into a large scale drilling scenario. Analysis techniques included pressure recordings, high speed video and PIV. Parameters for both Newtonian and non-Newtonian liquids were investigated.
These experiments are relevant for large scale flows in pipes in process industries as well as for drilling scenarios both onshore and offshore.

A numerical simulator was made by the use of Matlab in order to mathematically simulate the flow behavior in the system. This was done to bridge the gap between theory and the performed experiments. In the end, the complexity of the system with all its uncertain- and unknown parameters proved to be too much for the simulator and it was unable to yield accurate predictions of the flow behavior.

TABLE OF CONTENTS

1. INTRODUCTION

Drilling always involves the use of mud, whether it is onshore or offshore. The mud is injected at the drilling bit through the string and serves several purposes, such as pressure control, lubrication, downhole cleaning, and to prevent overheating. The topic is described in detail by Saasen et al[1].
A risk drillers face is the occurrence of highly pressurized gas zones while drilling. Under poor pressure control, gas may invade the well and mix with the present mud. If gas accumulates in the annulus it may cause a hydrostatic pressure difference between the drilling-string and the surrounding annulus. In scenarios like this, severe oscillation as seen in U-tubes may occur.
The gas will continue to travel up the well, expanding as the pressure decreases. This is a recipe to what is known as a gas-kick. When gas escapes from the well onto the rig, disasters such as the Macondo incident in 2010 on the Deepwater Horizon become a reality.

In order to get a better understanding of this gas kick phenomenon, this thesis is dedicated to study oscillatory movement of fluids in a U-tube. A rig was constructed with two vertical pipes simulating the drill-string and annulus. Injecting a pocket of gas in one of the vertical pipes will simulate a gas-kick. The pressurized gas bubble is kept stationary under a valve. When the pressure is equalized, the gas volume will adjusts itself under the hydrostatic weight from the adjacent column. The gas and liquid will oscillate by compression and decompression of the gas bubble. The system will come to a rest when the pressure is equalized and all the energy is dissipated from the system.
Another experiment was conducted without a gas-kick scenario. In this experiment, a height difference was made between the two risers, and then the fluid was set in motion and allowed to oscillate freely. Pure U-tube oscillations like this may occur during well start-up, casing-installation, string extraction or during gas-lift operations. The aim of studying and observing these fluid motions is to get a better understanding of fluid friction in complex geometries.

A numerical model was made in order to simulate the gas bubble response during the oscillation under the influence of the hydrostatic liquid column. Another one was made to simulate the oscillating fluid motion in the pure U-tube. The results gained from the simulator are compared with the observations seen in the experimental work.

Another aspect of this thesis is to study to what extent rheological data found in a lab can be used to give realistic predictions of flow in large scale complex systems.
The goal of this thesis is to provide information on the challenges that occur when such flows are to be modeled.

2.THEORY

2.1 Velocity Profile in Oscillating Pipe Flow. Simplified Navier-Stokes Equations

The Navier-Stokes assumption for the friction forces is purely empirical. One cannot be sure that the Navier-Stokes equations correctly describes the motion of a fluid. Therefore they must be checked, something that can only be done experimentally. It must, however, be taken into account that the great mathematical difficulty of these equations means that only very few solutions are known where the convective terms interact quite generally with the friction terms. The task of finding exact solutions of the general Navier-Stokes equations is generally extremely difficult. In spite of this, there are some special cases where exact solutions can be given, and this is the most often true when the nonlinear internal terms vanish in a natural way. Schlicting[2]

An exact solution of the Navier-Stokes equations may be found in long circular pipes. Let ***x*** be the coordinate along the axis of the pipe and ***r*** the radial distance from the centre. Since we assume that the pipe is long, the solution will be independent of ***x***. Using the Navier-Stokes equations and neglecting no other terms:

$$\frac{\delta u}{\delta t} = -\frac{1}{\rho}\frac{\delta p}{\delta x} + \nu\left(\frac{\delta^2 u}{\delta r^2} + \frac{1}{r}\frac{\delta u}{\delta r}\right) \qquad (1)$$

With the boundary conditions ***u(r=R,t) = 0*** (no-slip conditions). For the harmonically oscillating pressure gradient

$$-\frac{1}{\rho}\frac{\delta p}{\delta x} = K\,Sin\,nt \qquad (2)$$

One obtains the solution

$$u(r,t) = -\frac{K}{n}e^{int}\left[1 - \frac{J_0\left(r\sqrt{\frac{in}{\nu}}\right)}{J_0\left(R\sqrt{\frac{in}{\nu}}\right)}\right] \qquad (3)$$

Here J_0 is the zeroth order Bessel function. For very low frequencies we thus find the *quasi-steady* solution

$$u(r,t) = -\frac{K}{4\nu}(R^2 - r^2)Sin\,nt \qquad (n \to 0) \qquad (4)$$

At very high frequencies we have

$$u(r,t) = \frac{K}{n}\left[cos\,nt - \sqrt{\frac{R}{t}}\,e^{-h_s}\,cos(nt - h_s)\right] \qquad (n \to \infty) \qquad (5)$$

Where

$$h_s = \sqrt{\frac{n}{2\nu}}\,(R - r) \qquad (6)$$

This is again a solution with a two-layer structure: the inviscid core flow and the Stokes layer close to the wall. Fig.1 shows the velocity-profile of the oscillating pipe flow for an intermediate frequency ($\sqrt{\frac{n}{\nu R}} = 5$) at different times during one period of oscillation. Comparing the pressure gradient depicted below this, we can clearly see the phase lag of the flow in the centre of the pipe behind that in the layer close to the wall.

Pipe start-up flow is closely related to oscillating pipe flow. Here the fluid in the infinitely long pipe is initially at rest, at time *t = 0,* a time-independent pressure drop is suddenly switched on. Because of the friction and inertial forces, a pipe start-up flow forms which asymptotically passes over to the Hagen-Poiseuille parabolic velocity distribution. The characteristic here is that the velocity in the centre of the pipe initially remains locally almost constant, and the viscosity only has any effect in a thin layer close to the pipe. Only later does the action of the viscosity reach the center of the pipe. This is described in more detail in Schlicting[2] and Libii[3], citing Uchida[4].

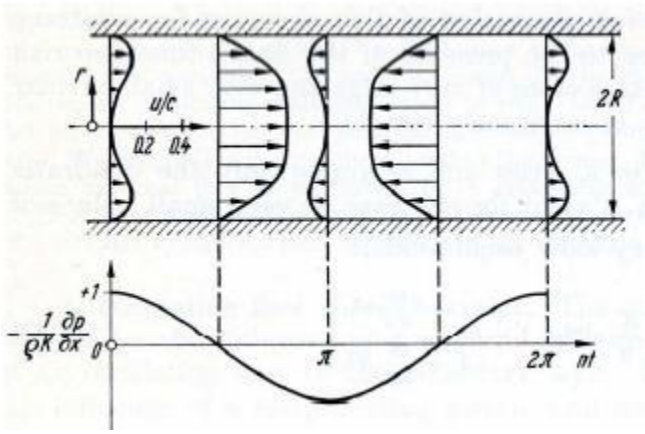

Figure 1: Velocity Profile in an Oscillating Flow as described by Uchida[4].Schlicting[2] page-141.

2.2 Polimers showing shear-thinning behavior. The entanglement model

Polimers such as CMC (Carboxy-Methyl-Celluloce) and PAC (PoliAnionic Celluloce)will form long chemical chains. These macromolecules may be used to describe why a fluid is considered shear-thinning. Using a illustrative dimensional comparison, these chains corresponds to a piece of spaghetti, which is 1mm thick, beeing 2m long. So, in shear thinning fluids, there are hundreds of thousands, even millions of these chains. These molecules will entangle loosely with others, creating a web of connected molecules. At rest, each single macromolecule can be found in the state of the lowest level of energy consumption: Without external load it shows the shape of a three-dimensional coil.
Each coil shows an approximately spherical shape and each one is entangled many times with neighbouring macromolecules. Mezger[5]

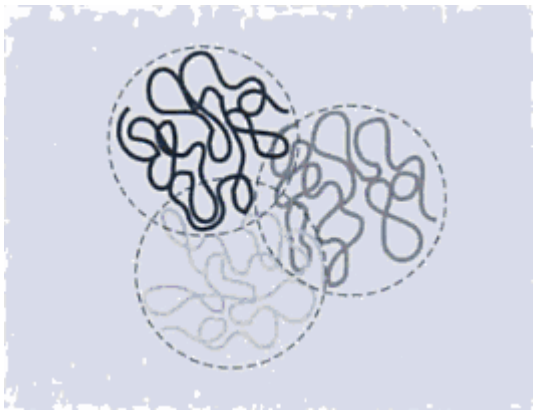

Figure 2: Three macromolecules at rest, showing coiled and entangled chains. Mezger[5]page-35.

During the shear process , the molecules are more or less oriented in the shear direction(influenced also by the shear gradient). In doing this, the molecules disentangle ro a certain extent, which lowers their flow ressistance. For very low concentrated polymer solutions, the chains may even become completely disentangled.

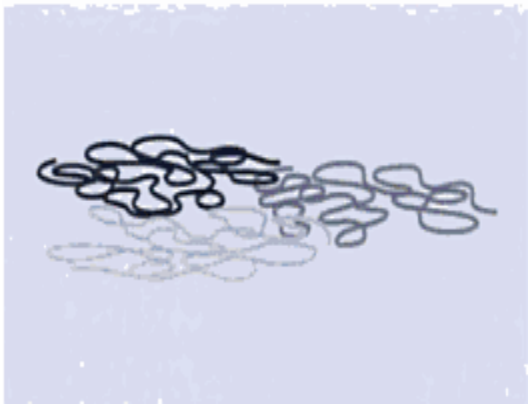

Figure 3: The same macromolecules under high shear load, showing oriented and disentangled chains. Mezger[5]page-36.

Fig.4 presents the viscosity function of a polymer showing three ranges on a double logaithmic scale. These three distinct ranges of the viscosity curve only occur for unlinked polymers with entangled macromolecules. However, this does not apply for polymer solutions showing a concentration which is too low to form entanglements, and also not for gels and pastelike dispersions showing a network of chemical bonds or physical interactive forces between the molecules or particles. The three ranges in detail:

(1) The first Newtonian range with the plateau value of the zero-shear viscosity η_0.

(2) The shear-thinning range with the shear rate-dependent viscosity function η**=f(**γ**°)**

(3) The second Newtonian range with the plateau value of the infinite-shear viscosity $\eta\infty$.

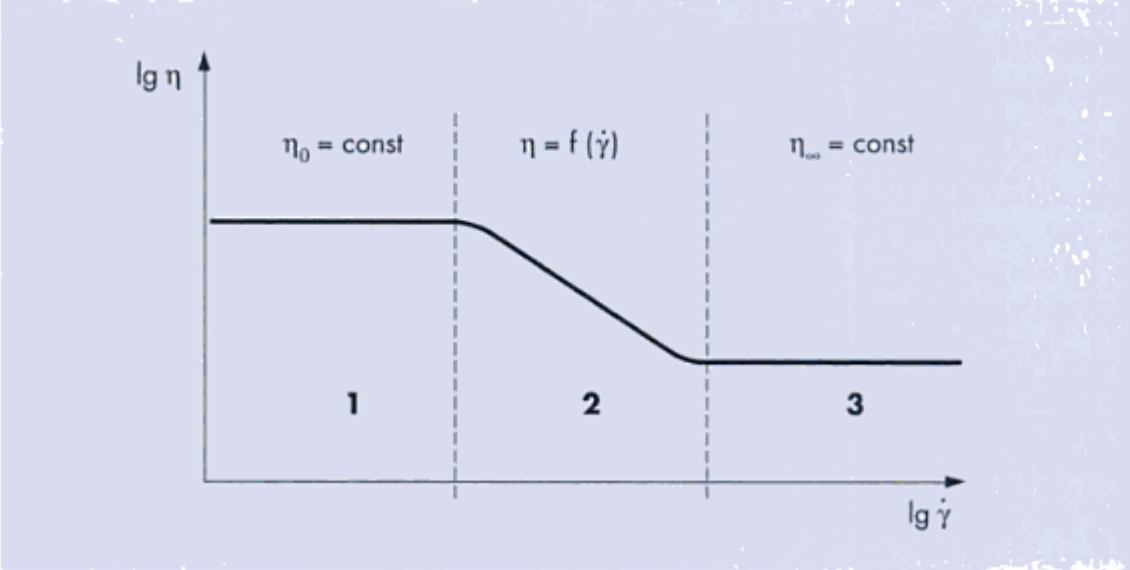

Figure 4: Viscosity functiosn of a polymer depicting the three different ranges. Mezger[5]page-36.

This topic is described in detail in Mezger[5].

Keep in mind that different authors often use different nomenclature when describing viscosity and shear forces.

2.3 Rheology Oscillatory Test

Oscillatory tests are used to examine all kinds of viscoelastic materials, from low-viscous liquids to polymer solutions and melts, pastes, gels, elastomers, and even rigid solids. This mode of testing is also referred to as “dynamic mechanical analysis” (DMA).

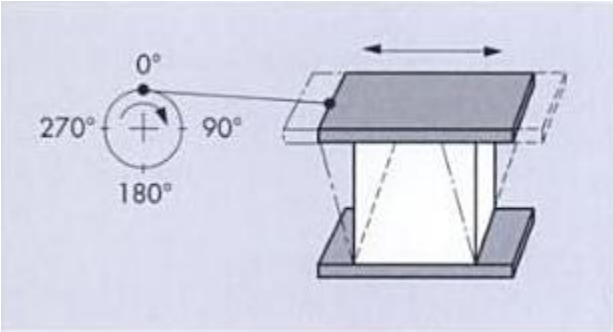

Figure 5: Oscillatory shear test using two plates. Mezger[5]page-114.

Fig.5 illustrates how the oscillatory motion of the upper plate might be produced mechanically by a drive wheel. A rod is connected eccentrically with the wheel at the one end, and with the upper plate at the other end. The bottom plate is stationary. When the wheel is turning, the upper plate with the shear-area (**A**) is moved back and forth by the shear-force (±**F**). The distance (**h**) between the plates is the shear-gap dimension. The motion of the upper plate causes shearing of the sample which is placed between the two plates showing the deflection path (±**s**) and the deflection angle (±**ϕ**). It is assumed that the following shear conditions are kept:

1) The sample adheres to both plates and does not slide or slip along them.
2) The sample is deformed homogeneously throughout the entire shear-gap.

Then, the shear stress: **±τ [Pa] = ±F/A**, And the shear strain (deformation): **±γ = ±s /h = ±tan φ.** Mezger[5].

2.4 Fast Fourier Transform (FFT)

A Fourier transform is a numerical algorithm which converts time to frequency and vice versa. An example of this conversion is given in Fig.6. A FFT is a computer algorithm which does so rapidly. They are widely used for many applications such as engineering, science and mathematics.

The algorithm is used to compute the Discrete Fourier Transform (DFT) and its inverse. The DFT is obtained by decomposing a sequence of values into components of different frequencies. Computing these DFT directly from the definition is often time consuming. The difference in using FFT can be enormous, especially for long data sets where *N* may be in the thousands or millions. The most common FFT algorithms depend upon the factorization of *N. FFT*[6].

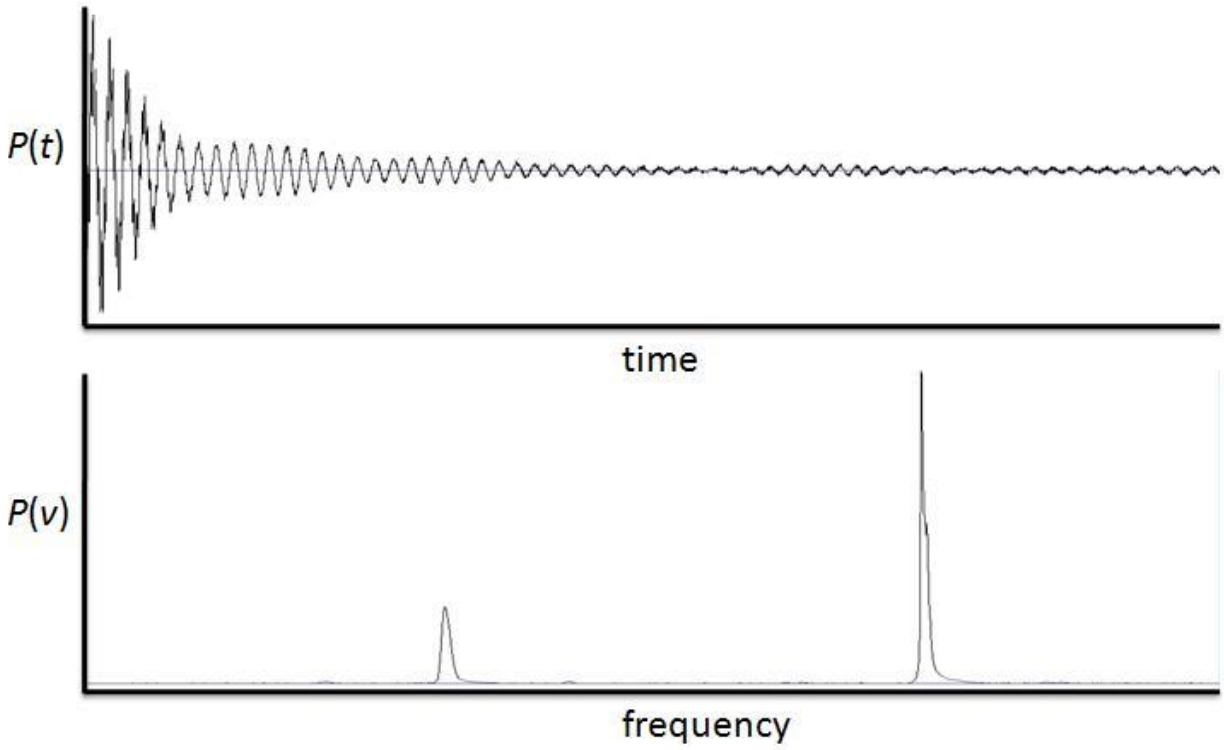

Figure 6: An example of how a Fourier algorithm converts time into frequency, http://en.wikipedia.org/wiki/File:Time_domain_to_frequency_domain.jpg Uploaded by user Pbchem 3 July 2011.

2.5 Particle Image Velocimetry (PIV)

PIV is a non-intrusive laser optical measurement technique for research and diagnostics into flow, turbulence, microfluids, spray atomization and combustion processes. Standard PIV measures two velocity components in a plane using a single camera. It is also possible to add an additional camera and obtain a Stereo PIV which measures three velocity components. The principle behind PIV is to derive velocity vectors from sub-sections of the target area of the particle-seeded flow by measuring the movements of particles between two light pulses:

$$\bar{V} = \frac{\Delta \bar{X}}{\Delta t} \qquad (7)$$

The flow is illuminated in the target area with a light sheet provided by a laser. The camera is able to capture each light pulse in a separate image frames. Each image is cross-correlated with each other, pixel by pixel. The correlation produces a signal peak, identifying the common particle displacement. An accurate measure of this displacement – and thus also the velocity – is achieved with sub-pixel interpolation. A velocity vector map over the whole target area is obtained by repeating the cross-correlation for each interrogation area over the two image frame captured by the camera.
Below, in Fig.7, an example of a velocity vector map is given. Notice how the PIV clearly shows the vortices in the flow. Dantec[7]

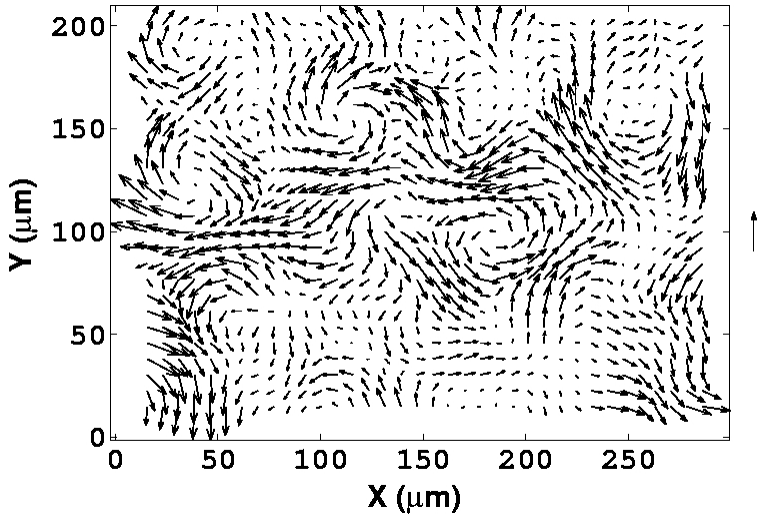

Figure 7: A velocity vector map obtained through a PIV analysis http://www.physics.arizona.edu/~cisneros/publications.html. Cisneros[8]

3. EQUIPMENT

3.1 Differential Pressure Sensor

In order to detect and transmit any pressure-alteration in the facility, the transmitter of the type "Rosemound 3051" was used and is depicted below.

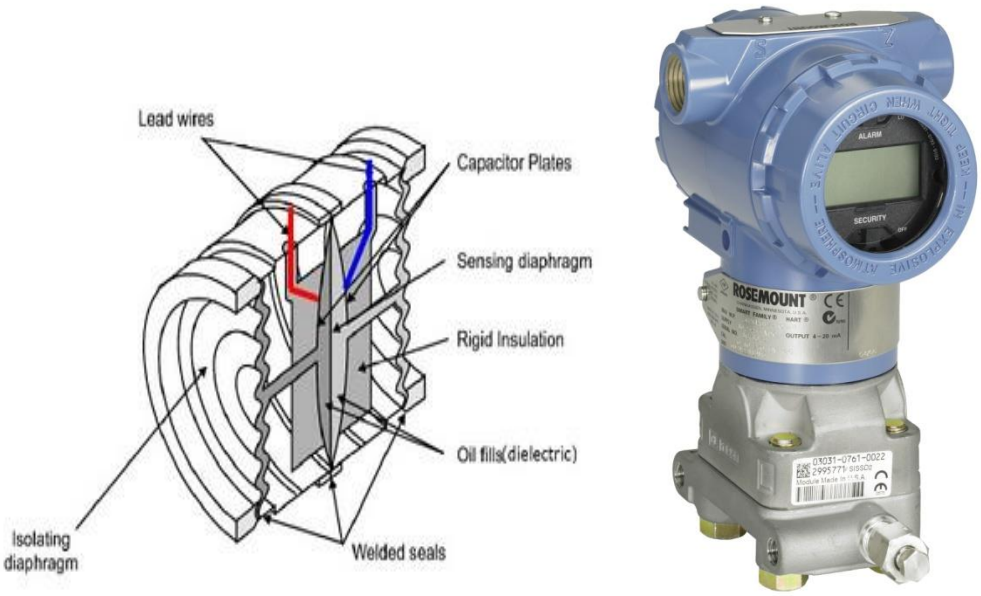

Figure 8: A basic schematic of a differential capacitance pressure sensor; http://instrumenttoolbox.blogspot.no/2011/02/electrical-pressure-sensors-used-in_13.html "
The Rosemound 3051 Pressure Transmitter; "http://www2.emersonprocess.com/en-us/brands/rosemount/pressure/pressure-transmitters/3051-pressure-transmitters/pages/index.aspx[10]

The Rosemound pressure-sensing device uses capacitance to detect any pressure-alteration between two systems, or one system and the atmosphere. It is a differential capacitance pressure sensor.
The principal functionality of this device is that any difference in pressure across the cell will cause the diaphragm to flex in the direction of least pressure. This results in a change of capacitance across the cell. A high frequency capacitance detector circuit connected to this cell uses a high-frequency AC excitation signal to measure the difference in capacitance between the two halves, translating that into a 4-20mA DC signal which then becomes the signal output by the instrument representing pressure. Differential capacitance sensors are highly accurate, stable and rugged. They have a wide operating range. Their solid frame bounds the motion of the two isolating diaphragms such that the sensing diaphragm cannot move past its elastic limit. This gives the differential capacitance sensor excellent resistance to overpressure damage. "Differential Capacitance Pressure Sensors" [9]

3.2 High Speed Camera

A camera of the sort “SpeedCam MiniVis-e2” was used in the experiments to monitor the movement of the liquid interface. The recordings were also used in collaboration with a PIV program to calculate the velocity profile. The camera has a limit of 2500 fps (frames per second) and a 512x512 pixel resolution. It may record up to 120.000 fps albeit at lower resolutions.

Images are transferred to a computer using a dedicated interfacing program (“MotionBlitz” by Mikrotron). For the PIV recordings a continuous wave (CW) diode laser (type “Suwtech”) was used. It gives a beam with adjustable energy up to 200mW, and fixed wavelength of 532nm. By the use of a cylindrical lens in sequence with a collimator lens, the laser beam was expanded into a 1mm thick and 5cm wide, nearly parallel “light sheet”.

Figure 9: Pictures of the diode Laser and the High Speed Camera. Photographed by Kim Flatråker.

3.3 Rheometer

A rheometer is a laboratory device used to measure the way in which a liquid flows in response to applied forces. It is used for those fluids which cannot be defined by a single value of viscosity and therefore require more parameters to be set and measured than is the case for a viscometer. It measures the rheology of the fluid. The word “Rheology” originates from Greece and its literal translation is “Flow Science”. Mezger[5].

For this purpose, the apparatus “Anton Paar MCR 302” has been used. It is a sophisticated rotational shear rheometer, with air-bearing-supported synchronous EC motor, a dynamic TruRate™ sample-adaptive motor controller and a normal force sensor integrated in the air bearing, TruStrain™ real-time position control. For more information on the rheometer, visit Anton-paar.com. Anton Paar[11].

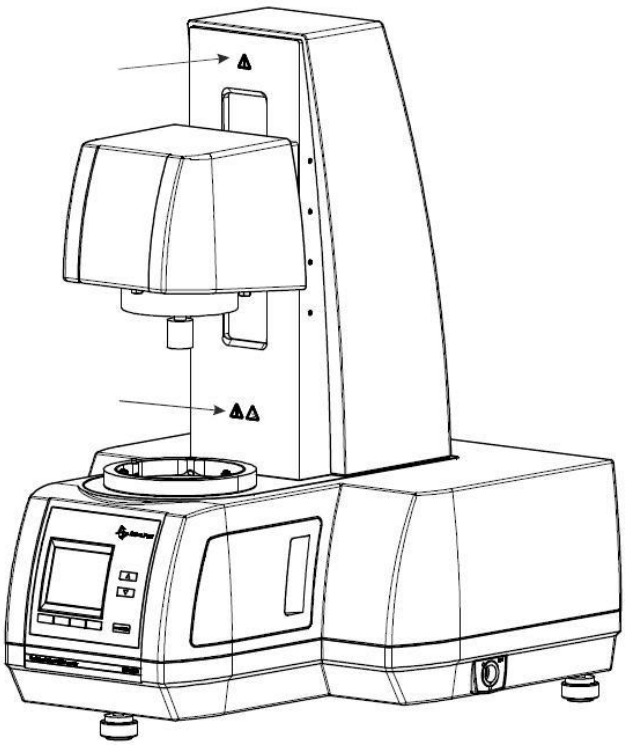

Figure10: the Anton Paar MCR-302 Viscosity Meter .Anton Paar[11] page-12.

A Carreau-Yasuda model is often used to describe CMC. The model describes a fluid where viscosity,(μ_{eff}), depends upon the shear rate,(γ), by the following equation:

$$\mu_{eff}(\gamma) = \mu_{inf} + (\mu_0 - \mu_{inf})\,(1+ (\lambda\gamma)^a)^{((n-1)/a)} \qquad (8)$$

μ_0 = Viscosity at zero shear rate (Pa*s)
μ_{inf} = Viscosity at infinite shear rate (Pa*s)
λ = Relaxation time (s)
n = Power index
a = Dimensionless parameter

At low shear rate (γ <<1/ λ) a fluid behaves as a Newtonian fluid and at high shear rate (γ >>1/ λ) it has a power-law characteristic. The power-law index for shear-thinning fluids is always below one (n<1) as described in more detail in Kennedy[12].

3.4 Density meter

In order to determine the liquid density, an Anton-Paar DMA 4500 was used. The DMA 4500 is the first oscillatory U-tube density meter and measures with highest accuracy in wide viscosity and temperature ranges. It was quite fitting to be using an oscillatory U-tube density meter in this thesis. By measuring the damping of the U-tubes's oscillation caused by the viscosity of the filled-in sample, the DMA 4500 automatically corrects viscosity related errors. Two integrated Pt 100 platinum thermometers provide highest accuracy of temperature control. The accuracy of the density meter is $5*10^{-5}$g/cm^3. Anton Paar DMA-4500[13].

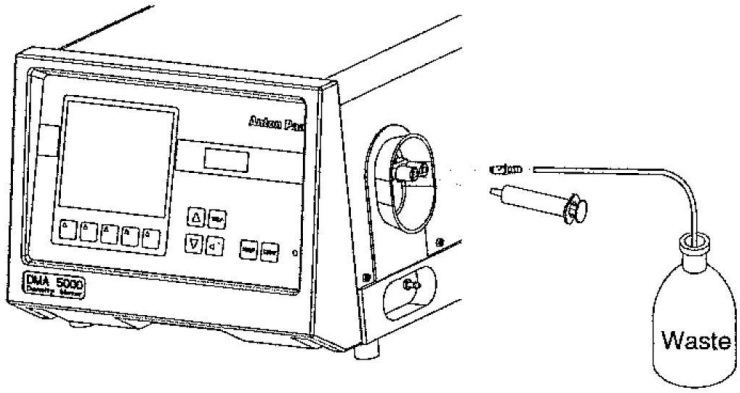

Figure 11: The Anton Paar DMA-4500 Density Meter. Anton Paar DMA-4500[13] page-33

4. EXPERIMENTAL SECTION

4.1 Density Measurements

When using the Anton Paar DMA 4500, there were some factors to keep in mind. Correct temperature adjustment was important. 20°C was used for all three liquids. To make sure that no residue is left behind from any previous measurements, the apparatus was thoroughly cleaned and dried.
In order to measure the density, the sample was injected into the measuring cell by the use of a syringe. The U-tube was visible through a display window and it was then easy to ensure that no gas bubbles were present in the sample. When the sample was in place, the "Go" button was pushed and after roughly 30 seconds, the density of the sample was visible on the display. Afterwards, the measuring cell was cleaned and dried. The density meter was easy and straightforward to operate. The results are shown in the table below.

Liquid (20°C)	Density (g/cm^3)	Specific Density (4°C reference)
Tap Water	0,9982	0,9982
1g/l CMC	0,9986	1,0004
10g/l CMC	1,0036	1,0054

Table 1: Showing the density of the three fluids.

The density is not critically affected by the addition of the CMC polymer, nor is it intended to. An Increase of 5% in the case of 10grams per liter. In an actual drilling fluid, bentonite and baryte clays are added to gain a higher liquid density. These weight particles are omitted in this work since they obscure vision through the liquid. It is important that the liquid is transparent for PIV measurements and video imagery of the interface between gas and liquid.

The CMC (of the type C5678 from Sigma Aldrich) has a molar mass of 90 g/mol.

Figure 12: Picture of the Density meter as it is measuring the 1g/l CMC. Photographed by Kim Flatråker.

4.2 Rheological Experiments

The rheological experiments were performed with the MCR-302. This apparatus had a lot of different configurations and properties. All of the experiments were run at 20°C to keep them consistent. The MCR-302 is a very sophisticated piece of machinery, and had to be handled with utmost care. For the experiments conducted, the plate-cone (CP50-1) modification was used, which has a separation distance of 0.096mm. The learning-curve for the rheometer was very steep, and a lot of time was spent on gaining knowledge on how to operate it before any results were made. Countless tests were done before any satisfactory results were had, and each test was also quite time-consuming.
Both a rotational shear tests and oscillatory tests have been performed. For the shear tests, the results seem to follow the Carreau-Yasuda Model, in respect that at high and low shear-rate, the viscosity is constant. Although, focus was not directed towards the lower shear-rates, therefore a perfect match to the Carreau-Yasuda Model was not feasible. It is also worth mentioning that at extremely high shear-rates, the fluids will actually gain a shear-thickening effect. This was tested and is shown Fig.17. It was only tested in the 1g/l CMC concentration, because at such high RPM, liquid was literally spun off the plate. For further studies on higher shear rates, another modification of the rheometer is recommended.

Figure 13: Picture of the Anton-Paar MCR-302 Rheometer

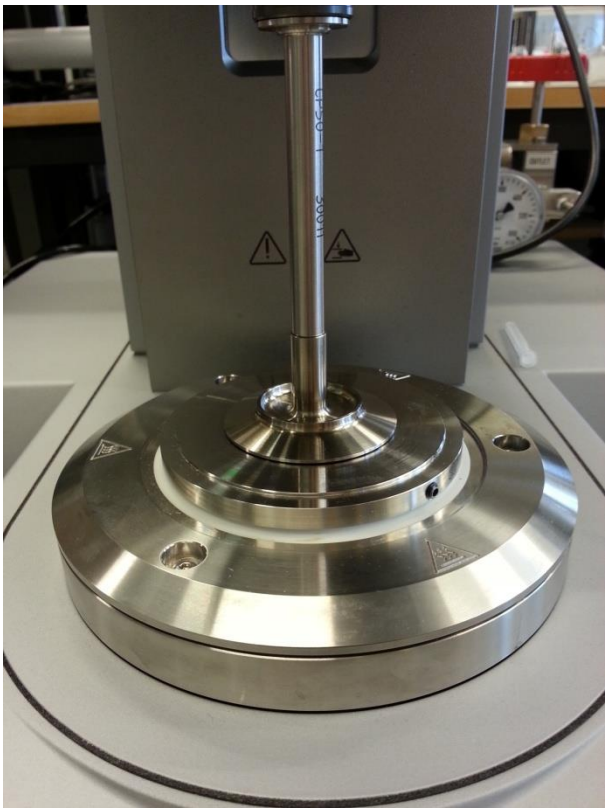

Figure 14: A close-up picture of the Plate-and-Cone (CP-50-1) configuration at measuring position.

Photographed by Kim Flatråker.

4.2.1 Rotational shear test

The tests were performed by applying the sample liquid to the measuring plate by a syringe. For the cone -plate configuration it is very important that the liquid sample is just outside the rim of the measuring system, as shown in Fig.15. Ideally, all the excess sample should be removed at a position just above the measuring position. Both too much and too little sample will lead to large errors in the measuring data. The sampling process is the most important parameter when it comes to repeatability and accuracy of the experiments. This was not an easy task and a lot of test data, unfortunately, had to be discarded.

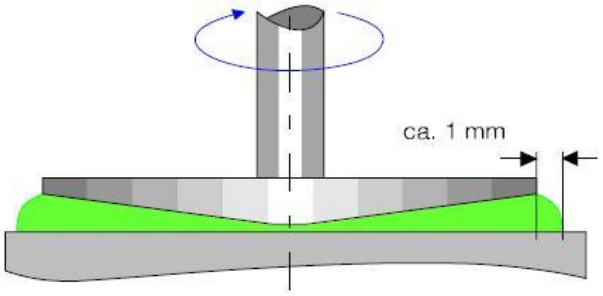

Figure 15: The Plate-Cone (CP50-1) configuration in its measuring position with ideal amount of sample present .Anton Paar[11] page-32.

When a satisfactory sample was placed and the system was in the measuring position the test could start. The whole process was controlled from a connected computer. The tests were run with a Shear ramping option. The amount of measuring points was set to roughly 30 (some tests with more, some with less). The rheometer then spent 10 seconds per measuring point and reported back the mean value of those 10 seconds for each test. Most of the tests were run from a shear rate of 0.01/s up to 1000/s and then back from 1000/s down to 0.01/s again.

In Fig.16, the results from the shear tests are shown. Water is added to the plot as a reference and to give an intuitive comparison to the CMC. The 1g/l test starts with a shear rate of 0.01/s and a viscosity of 0.175Pa*s. From Mezger[5], a Newtonian "zero-shear" plateau was expected in these initial lower shear rates, where the viscosity would be unaffected by the shear rate. This was, for some unknown reason, not shown in this test. In Fig.17 on the other hand, a hint of a plateau is shown for the lower shear rates. Maybe if the test started at 0.001/s, a better Newtonian plateau would be visible.
As the test continues, the viscosity keeps a steady decline and is called the "shear thinning" range. The viscosity is intimately connected to the shear rate. When the shear rate reaches approximately 80/s, the 1g/l CMC reaches its "infinite-shear" plateau with a constant viscosity of 0.00142Pa*s. This viscosity value is quite close to that of water. This range is what Mezger[5] calls the second Newtonian range, where viscosity no longer is affected by the increasing shear rate. Out of curiosity, this statement was put to the test (as shown in Fig.17). In this test the shear rate was ramped up to 10,000/s, and after approximately 1500/s the shear thinning liquid exhibits shear thickening properties. Although very unexpected, this phenomenon was not investigated in any further detail.

In the case of the 10g/l CMC, the test starts with a shear rate of 0.1/s and a viscosity of 0.671Pa*s. This CMC concentration is 670 times more resistant to fluid motion compared to water, which is quite significant. No initial Newtonian plateau was shown for this test. The shear thinning range lasts until the shear range reaches its “infinite-shear” at roughly 100/s. From here, the viscosity is kept at a constant 0.0074Pa*s.

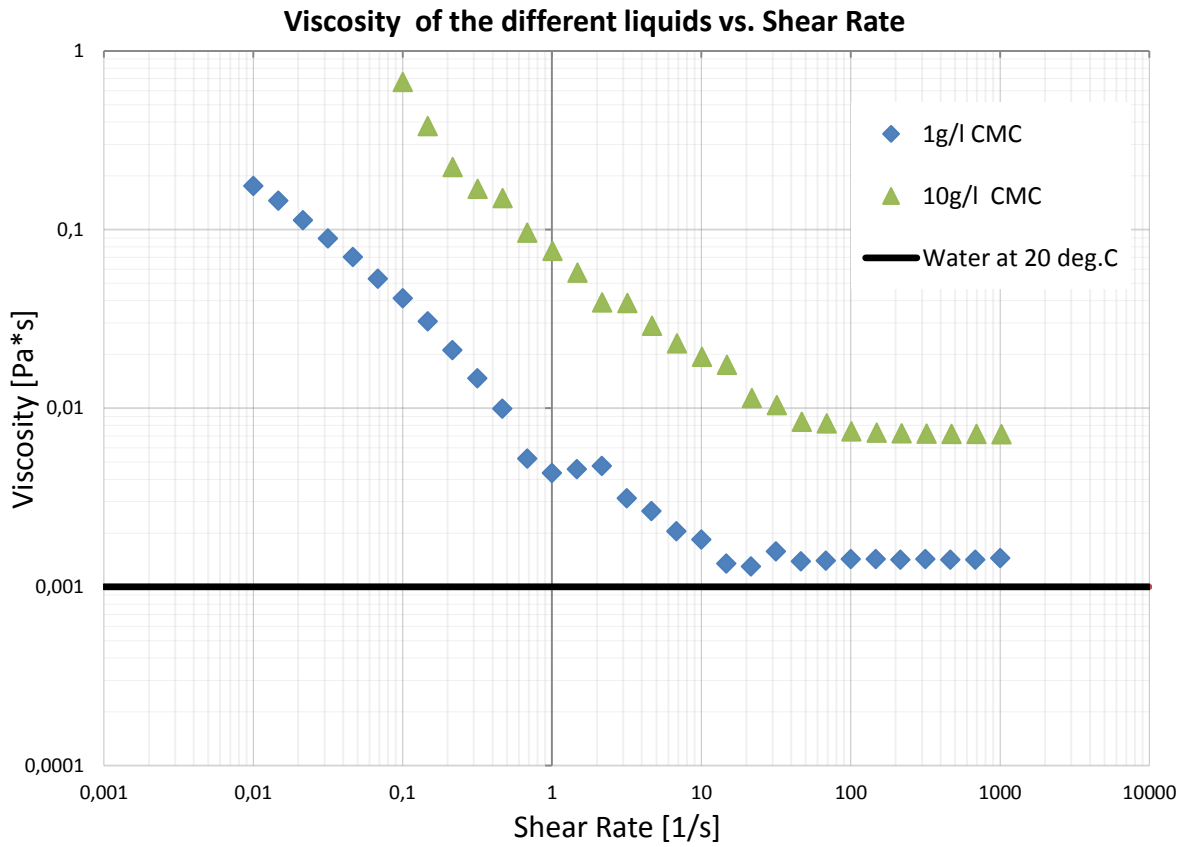

Figure 16: Rheology of the different liquids vs. the Shear Rate. Water inserted as a reference (1cP at 20°C).

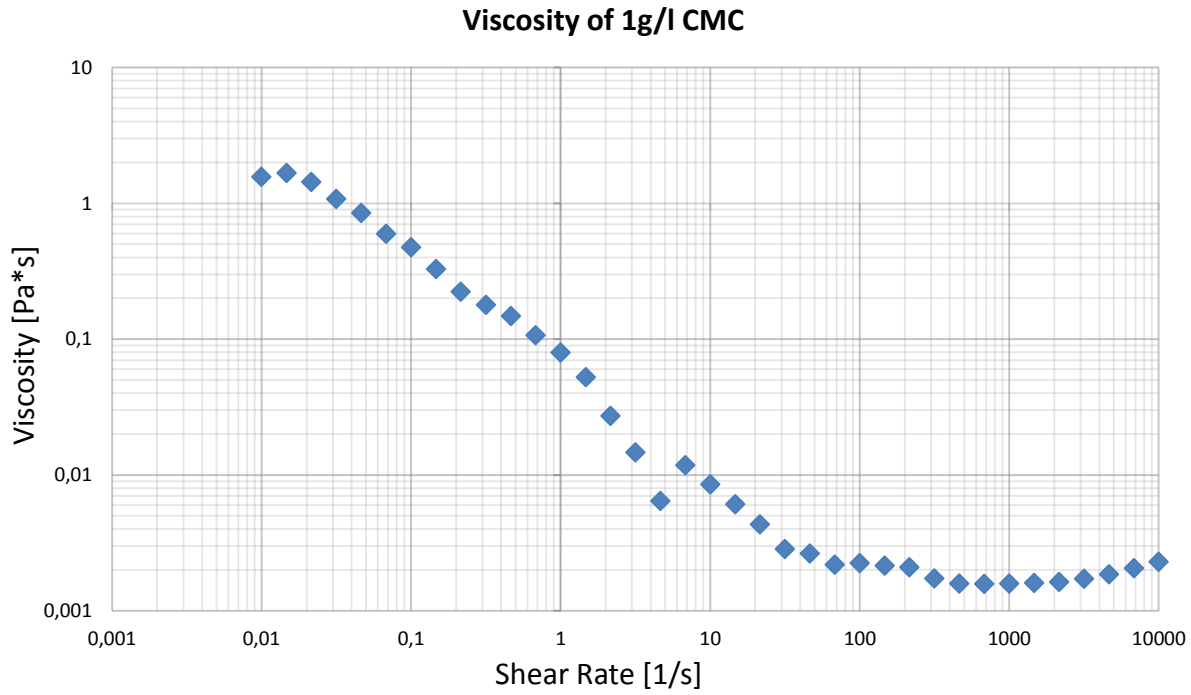

Figure 17: At extreme shear rates, the shear-thinning liquid exhibits shear-thickening properties.

One of the tests was showing strange behavior at the lower shear rates, and is given in Fig.18. Here it seems as if though the viscosity is dropping at the lower shear rates, but this is actually not the case. This is an example of what Mezger[5] calls a “transient viscosity peak”. These become present when the measuring point duration of the test is too low. For the test in Fig.18 a constant measuring duration per point was 10s, which evidently is too short. Mezger[5] recommends the use of a variable time range, starting with 120s per measuring point for the lower shear rates and decreasing this to 5s per point towards the higher shear rates.
Further investigation reveals that the transient viscosity peak actually is proof that the CMC exhibits viscoelastic behavior. This may also indicate that the CMC is forming a weak gel-like structure when no stress is applied to it. A gelling liquid is defined a colloid mixture that forms cohesive internal structures. In CMC, it is the long micro-molecular chains that adhere or interlock to resist strain.

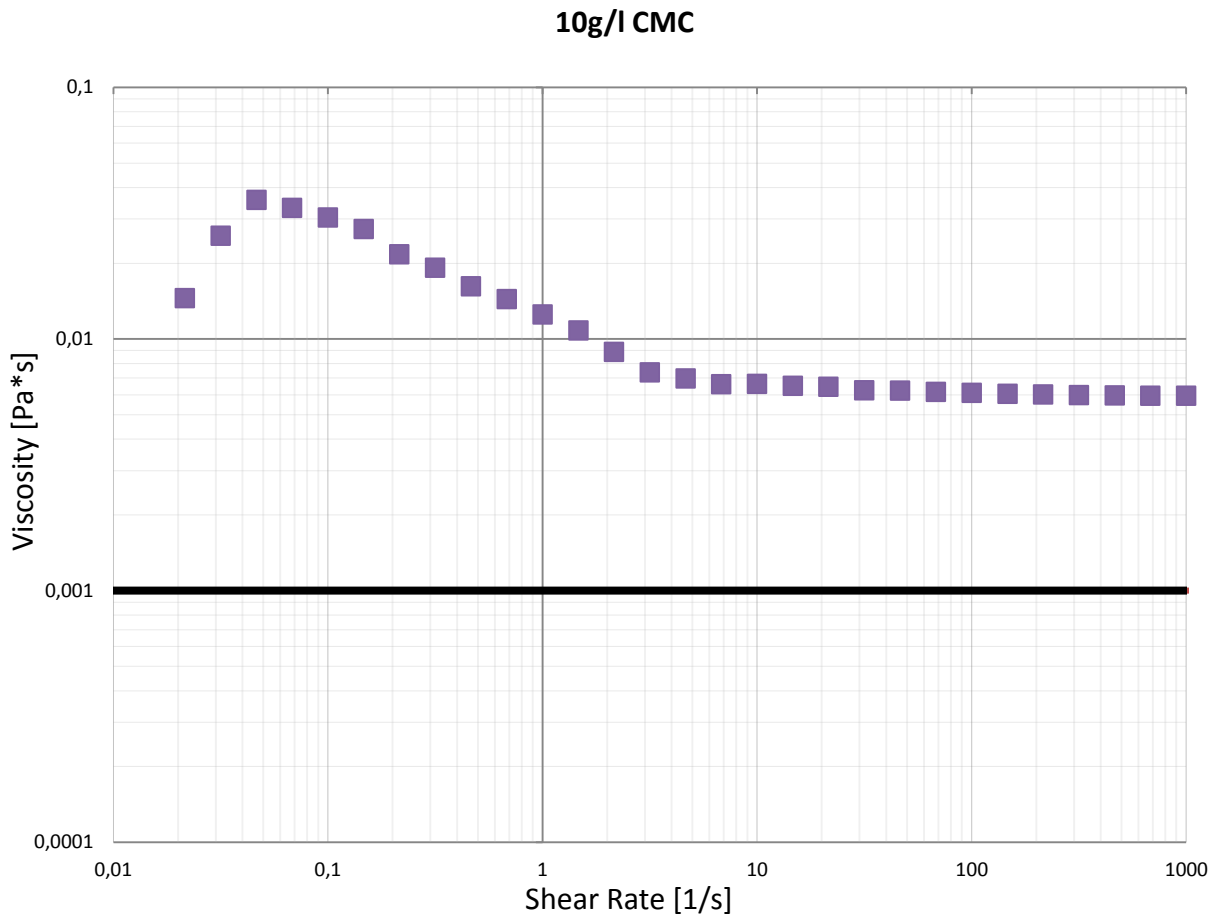

Figure 18: Shows the Transient viscosity peak, proving that the fluid yields gel-like viscoelastic structures.

The rheometer was always on a tight schedule, and booking time for testing was always an issue. Only after the tests were analyzed did it become apparent that more tests were needed. The rheometer was unfortunately not available for further testing.

For further information, the data tables for the tests are given in Appendix 9.

4.2.2 Oscillatory test

The tests were performed in the same manner as for the rotational shear tests, with the use of the (CP-50-1) plate-cone configuration. The tests were run from the computer with an amplitude sweep option. The strain (deformation) was ramped from 0.1 to 500% and the angular velocity was kept at a constant 3rad/s. In the case of the oscillation tests, as with the shear tests, a lot of trial and error went into the experiments before any satisfactory results were made. Different values of the angular velocity were also investigated, but they all showed the similar trend.

When performing oscillatory tests, a rheometer only measures two raw data. Torque and deflection angle in the case where the strain is preset. From these two independent variables, the viscous portion (G``) and the elastic portion (G`) of the viscoelastic behavior are determined.

The storage modulus, G`-value, is a measure of the deformation energy stored by the sample during the shear process. After the load is removed, this energy is completely available, now acting as the driving force for the reformation process which will compensate partially or completely the previously obtained deformation of the structure. Thus, the G` represents the elastic behavior of a fluid. Mezger[5]

The loss modulus, G``-value, is a measure of the deformation energy used by the sample during the shear process and is therefore lost for the sample. This energy is spent during the process of changing the material's structure, i.e. when the sample is flowing partially or altogether. Internal friction forces consume this energy and it is dissipated from the system. This process is also called "viscous heating". Thus, G`` represents the viscous behavior of a fluid. Mezger[5]

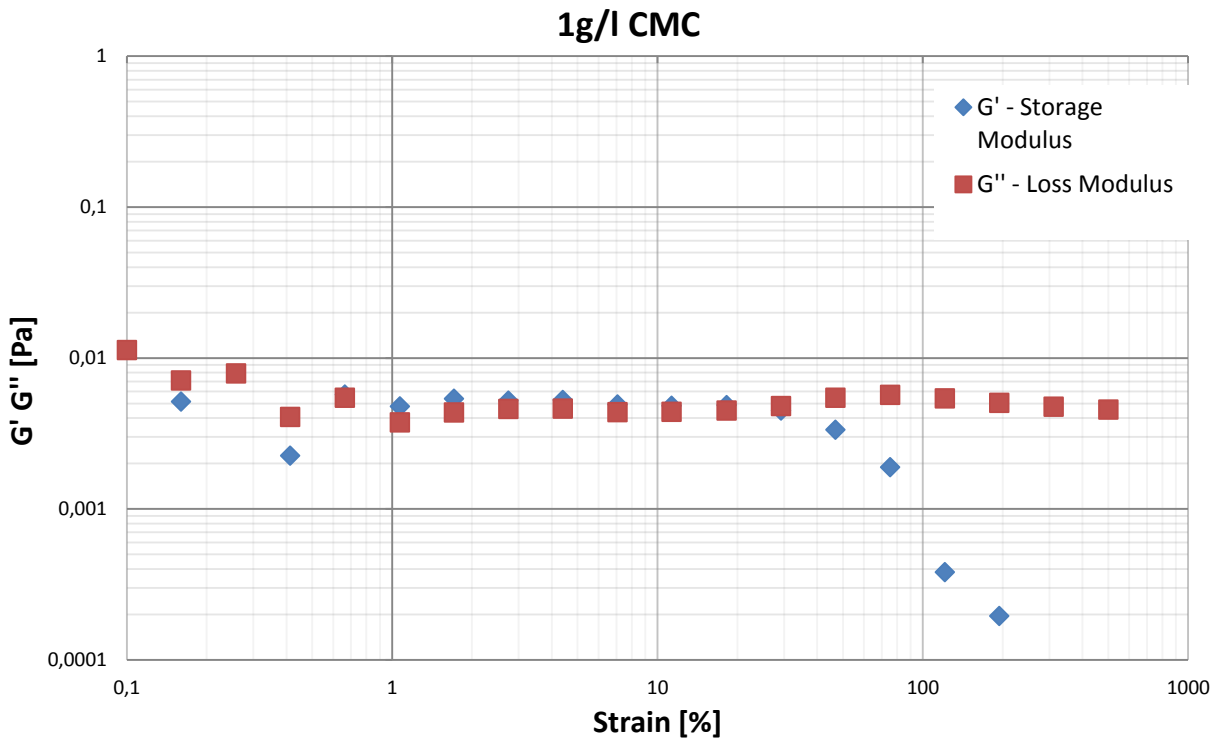

Figure 19: Showing the oscillatory test for the 1g/l CMC. Storage and Loss modulus are plotted vs. Strain.

The 1g/l CMC in Fig.19 exhibits a character where the elastic and viscous portions are equal until the storage (elastic) portion suddenly drops at roughly 50% strain. This means that the CMC is in a borderline between a liquid and gel-like in structure at lower strain. At higher strain, the energy is dissipated to the system and the fluid behaves more like a fluid without any gelling properties.

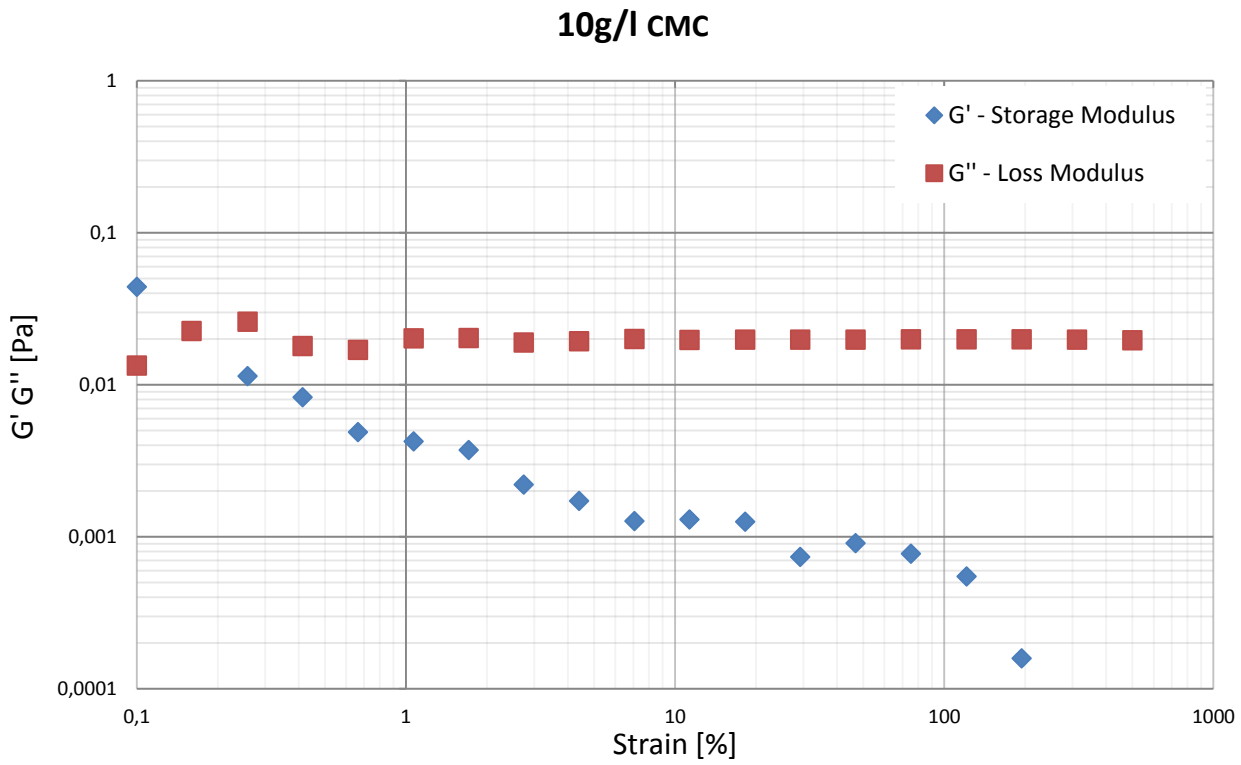

Figure 20: Showing the oscillatory test for the 10g/l CMC. Storage and Loss modulus are plotted vs. Strain.

The 10g/l CMC in Fig.20 exhibits a character where the viscous portion is greater than the elastic portion (G`` > G`). In this case, the viscous behavior dominates the elastic one. This is common in fluids that have a low- or no gel structure at low shear rates, which coincides with the results found in the rotational shear tests. Most of the energy is lost as viscous friction.
It is, however, worth mentioning that at the start of the oscillatory test, at low strain, that the elastic properties are greater than the viscous one. It would be interesting if a test was performed at even lower strain than 0.1%.

4.3 The Flow Rig Experiments

The most time consuming process of this work was the construction of the flow rig. Weeks and months of hard labor went into it. The most challenging part was the silicone insulator which was used to keep the acrylic pipes together and to prevent any leakage. This task proved more difficult than anticipated. In one incidence, a pipe joint burst open and 35 liters of water (luckily) flooded the lab. Small leaks were found frequently and they were very aggravating. If a pipe-connection was leaking, the whole pipe-segment had to be disassembled. This had a high risk of cracking and destroying the pipe (which unfortunately occurred quite often). Then silicone had to be sanded of, and a new layer of silicone applied before the parts were reassembled. The silicone used approximately two days in order to dry properly. Some of the parts even had to be custom made by the use of a lathe, which took quite some time as well. The flow rig was a modification of an existing facility made by Bachelor student Tomas Paz (2011).
This system is not a perfect U-tube by any stretch of the imagination, and is quite more complex with more bends and turns and even a change in pipe diameter. This is intentional, as to get a more in-depth understanding of flow behavior and the challenges faced when this is to be simulated.

When the rig was finally erected it was filled with water, roughly 35 liters. Afterwards, two different concentrations of CMC (Carboxy-Methyl-Cellulose) were studied, 1g/l and 10g/l respectively. Two different sets of experiments were conducted in the flow rig, namely the gas kick experiment and the pure U-tube experiment.
The basis of the gas kick experiments was to keep a static gas-pocket in one of the rising pipes, and then to apply hydrostatic pressure on the gas from the other pipe. This caused the gas to oscillate like a loaded spring before the volume and the pressure equalized.
The basis for the pure U-tube experiments was to create a liquid height difference between the two risers before the fluid was set in motion. The liquid oscillated back and forth until the energy in the system is dissipated.

The oscillation frequency is mainly connected to mass inertia and to gas compressibility, while amplitude decay can be related to liquid viscosity via friction. This oscillation was then studied and replicated in a Matlab simulation. Other authors such as Park[14] and Ogawa[15] also suggest the use of U-tube oscillations to measure rheological parameters.

The flow rig was also modeled with the software “Google Sketchup 3skeng” (3skeng was an engineering add-on). Quite some time and effort went into the making of this 3D model, especially since everything was done from scratch, nothing was known of modeling beforehand. This model is shown in Fig.21.

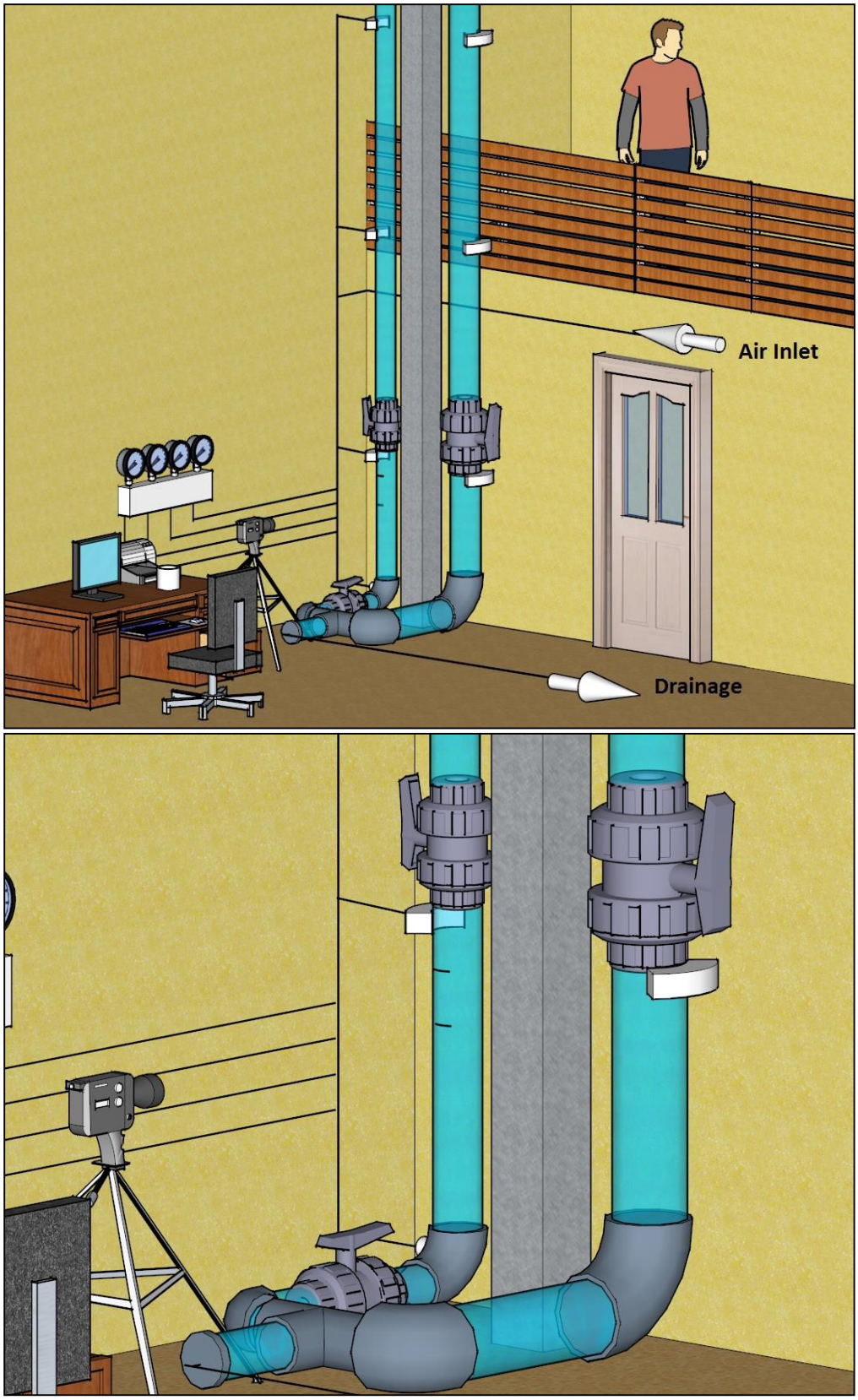

Figure 21: 3D model of the flow rig, created by Kim Flatråker using Google Sketchup.

4.3.1 Gas Kick Experiments

4.3.1.1 Initial setup for the Gas kick scenario

In order to keep the experiments comparable, they were all executed in the same manner. The setup is shown in Fig.22 in four simple steps.

A) A predefined amount of gas is introduced in the left pipe (i.d. 4cm) under the closed valve. The gas is trapped, creating a pocket. The valve in the right pipe (i.d. 8cm) is open as to allow the gas to displace fluid up the right pipe, creating a height differential between the two columns.

B) The right valve is then closed off, ensuring that the gas bubble still contains its volume and pressure. The overpressure under the valves is then bled off using a drainage hose located at the bottom. The bubble is allowed to expand while its pressure decreases to atmospheric pressure.

C) The drained fluid is poured back on top of the right pipe, increasing the height difference further. The hydrostatic pressure above the right valve is obviously higher than the pressure within the gas bubble. Mass conservation of the system dictates that if the right valve were to open, the system would return to its exact initial state.

D) The experiment is executed by opening the right valve. This will cause the gas bubble to compress and decompress in an oscillatory motion until pressure equilibrium is reached. It is this process of fluid motion we aim to study. The gas bubble has a huge damping effect and after roughly 10 seconds, the system is at rest.

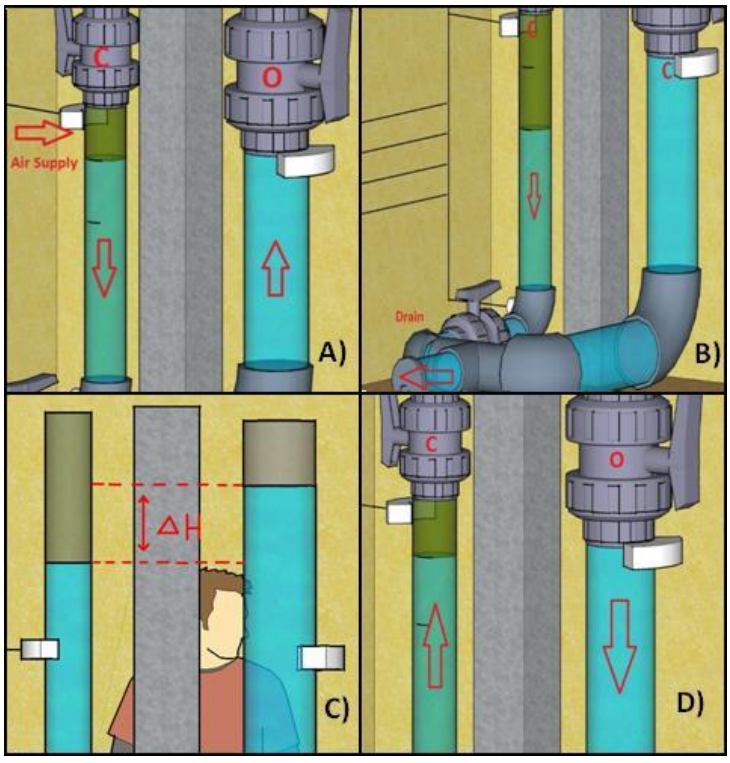

Figure 22: Shows how the experimental setup of the flow-rig. Created by Kim Flatråker using Google Sketchup.

This is the default setup for all the experiments.
Pressure sensors and high-speed camera were used to record the observations.

4.3.1.2 Gas kick experiment with Water

While the rig was water-filled, the experiments were conducted according to the described procedure. The volume of the pressurized gas pocket was 365 ml. When the two valves were closed and the pressure decreased, the gas pocket increased to 536 ml, now in standard conditions of 1 bar and 15°C. Fig.23 shows the transient oscillation of pressure vs. time. Pressure is given in gauge, relative to the ambient atmospheric pressure.

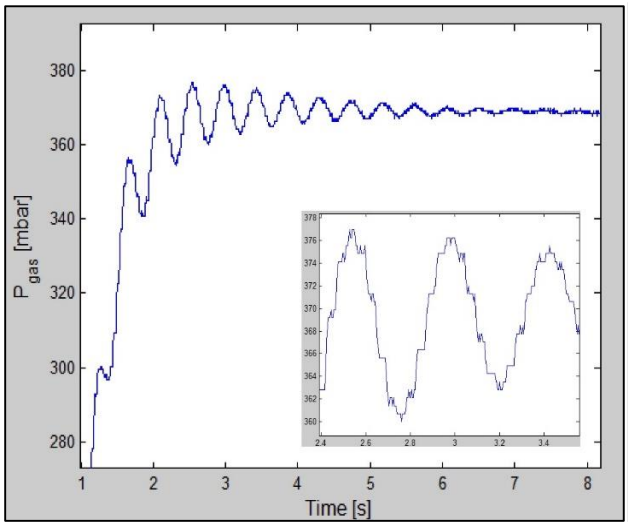

Figure 23: Water experiment: Pressure oscillations of gas with time.

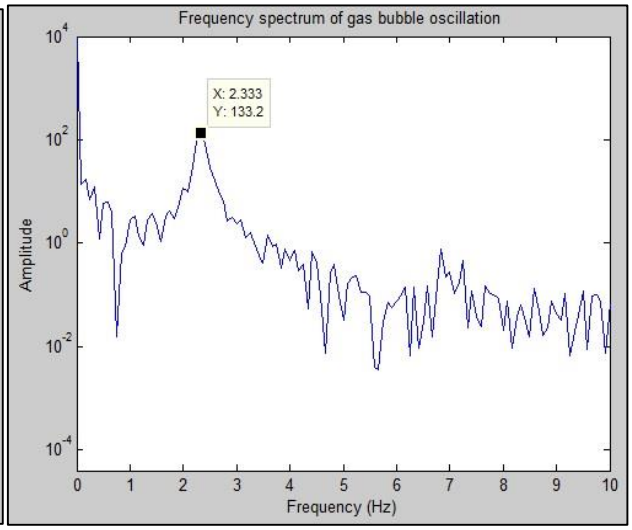

Figure 24: FFT Analysis, converting time into frequency.

At the moment the 8cm i.d valve is opened the computer software “Labview”, which records the pressure, is started. The initial pressure at in the gas is 0mbar (gauge). The pressure rapidly increases as the hydrostatic pressure propagates through the system. This propagation is not instant due to inertia. The maximum pressure of 334mbar is reached after 2.8 seconds. After rapid oscillation cycles, the pressure reaches equilibrium at 329mbar after roughly 10 seconds.
A Fast Fourier Transform (FFT) algorithm was applied to the pressure recordings in order to determine the oscillation frequency and is shown in Fig.24. The dominant frequency was 2.33 Hz, which coincides with the high speed video recordings. Another peak was seen at 20 Hz. This is connected to the update time of the pressure sensors. In the magnified pressure plot in Fig.23, this is clearly demonstrated by the jagged pressure behavior. This, however, should not be associated with the digital pressure resolution of the sensors (0.7mbar), nor with unwanted interference in the form of ambient electromagnetic “noise”.

In Fig.25, instantaneous images from the gas-liquid interface are shown as it passes the equilibrium level. The images were taken from the first oscillation cycle. Notice the time difference between the video images and the pressure recordings. They were both initiated at the same time. The first oscillation cycle starts at 0.219 seconds according to the video images, and at 1.4 seconds according to the pressure recordings. This is nothing but a time delay caused by human error. Investigation of the pressure recordings reveals that the pressure is a constant zero for 1 second before it suddenly rises, indicating that the program was started before the valve was opened.

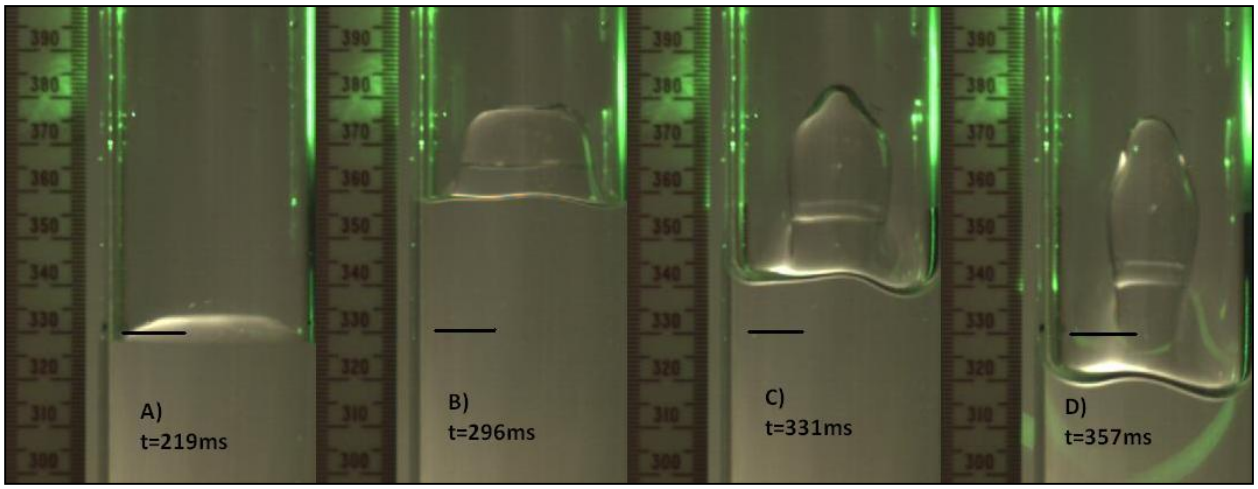

Figure 25: Depicts the first oscillation cycle of the water experiment.

A - 219ms) Interface as it passes the equilibrium line upwards.
B - 296ms) As the interface comes to rest, the core continues to rise.
C - 331ms) The liquid core reaches its maximum point and starts to decend.
D - 357ms) The distance between the interior core and the exterior wall increases further. The interface now crosses the equilibrium line, draining downwards.
Notice that the duration of the first cycle is only roughly 0.28 seconds long. Also, the interface reaches a maximum level of 55mm above the equilibrium line before the liquid starts to drain downwards.

Another interesting tidbit of information is how this relates what Uchida[4] found when studying oscillating flow in horizontal pipes. The effect of viscosity applies in the region close to the pipe wall first, and due to inertia some time passes before the center is affected. This causes the lagging of the pressure gradient vs. the velocity profile.

Since the following experiments on the CMC share many similarities with the water experiment, only the differences are highlighted. This is done to prevent any unwanted repetition of the same information three times over.

4.3.1.3 Gas kick experiment with 1g/l CMC

While the rig was filled with a CMC concentration of 1g/l, experiments were conducted with accordance to the described procedure. The initial volume of the injected gas bubble was 364 ml, and after the two main valves were closed and the pressure released to atmospheric pressure it became 534ml.
Fig.26 shows the transient oscillation of pressure vs. time. Pressure is given in gauge, relative to the ambient atmospheric pressure.

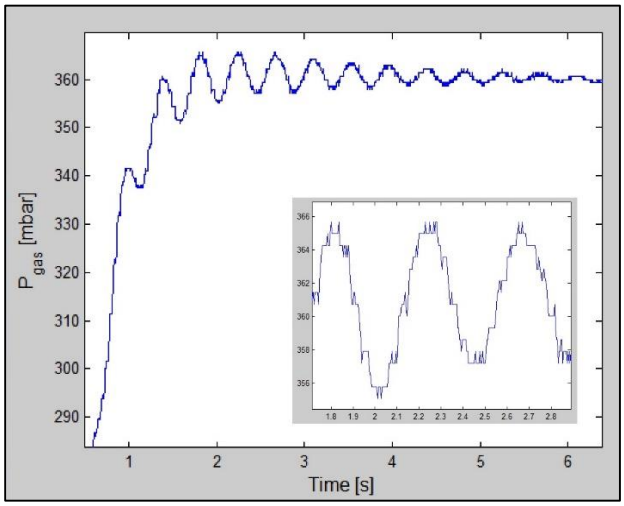

Figure 26: 1g/l CMC experiment: Pressure oscillations of gas with time.

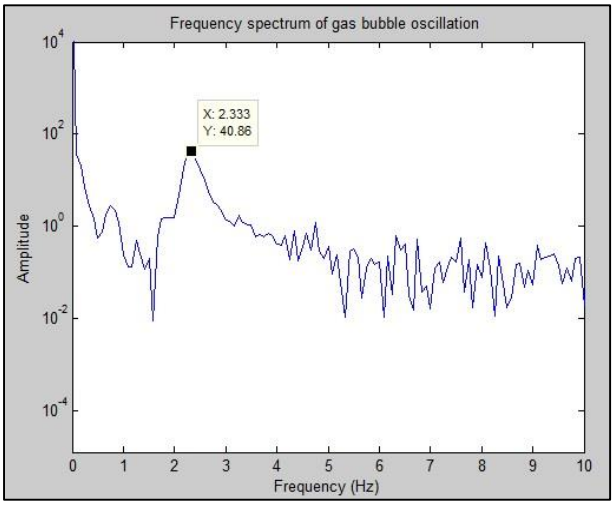

Figure 27:FFT Analysis, converting time into frequency.

The experiment starts with the opening of the 8cm i.d valve. The initial pressure is 0mbar and reaches its maximum of 366mbar after 1.8 seconds. After the pressure oscillations subside and equilibrium is reached, the pressure is 360mbar, which is the hydrostatic weight of the overlaying fluid column. The system is at rest after roughly 7-8 seconds.
The same FFT analysis (Fig.27) was applied in this experiment, the results was the same as for the water experiments. The dominant oscillation frequency was 2.33 Hz, meaning an average of 2.33 cycles each passing second. This is consistent with what is observed in the video images.

It is quite obvious from the video images provided in Fig.28 that the 1g/l CMC has a higher viscosity than water. The question is, by how much? In the light of the rheological shear test performed, the shear rate is in the shear thinning range, and have yet to reach the infinite-shear plateau. At higher shear rates, the liquid becomes less viscous and would behave more closely to water.

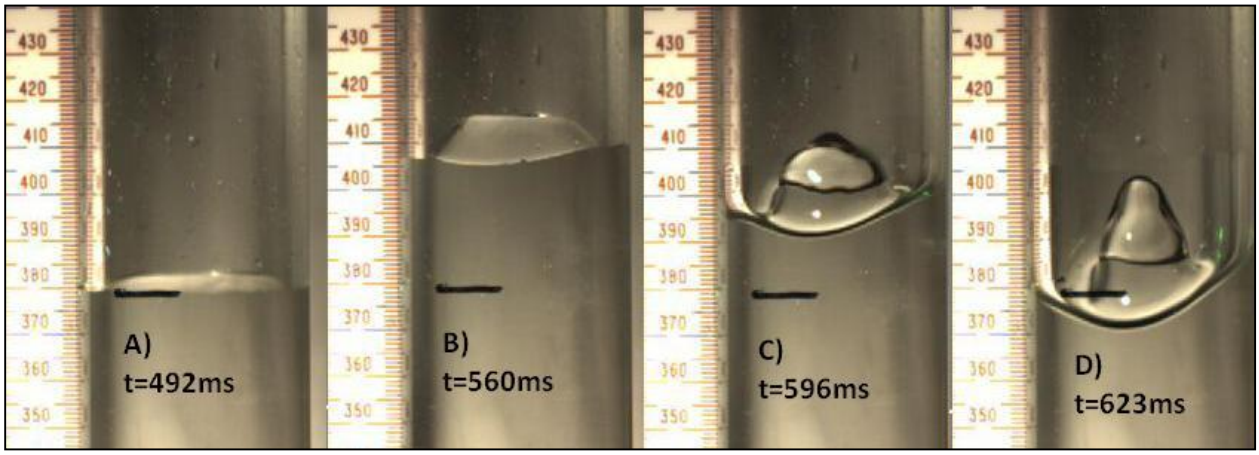

Figure 28: Depicts the first oscillation cycle of the 1g/l CMC experiment.

A - 492ms) Interface as it passes the equilibrium line upwards.
B - 560ms) As the interface comes to rest, the core continues to rise.
C - 596ms) The liquid core reaches its maximum point and starts to decend.
D - 623ms) The distance between the interior core and the exterior wall increases further. The interface now crosses the equilibrium line, draining downwards.
The maximum level of the interface is in this case reaches 35mm above the equilibrium line. The liquid Stalagmite is also much less distinct here compared to the one in the water. This is due to the increased viscosity.

4.3.1.4 Gas kick experiment with 10g/l CMC

As a final step for the flow rig experiments, the rig was filled with a CMC concentration of 10g/l. The experiments were conducted according to the described procedure. The initial gas bobble had a volume of 363ml, and after pressure release it expanded to 564ml. Fig.29 shows the transient oscillation of pressure vs. time. Pressure is given in gauge, relative to the ambient atmospheric pressure.

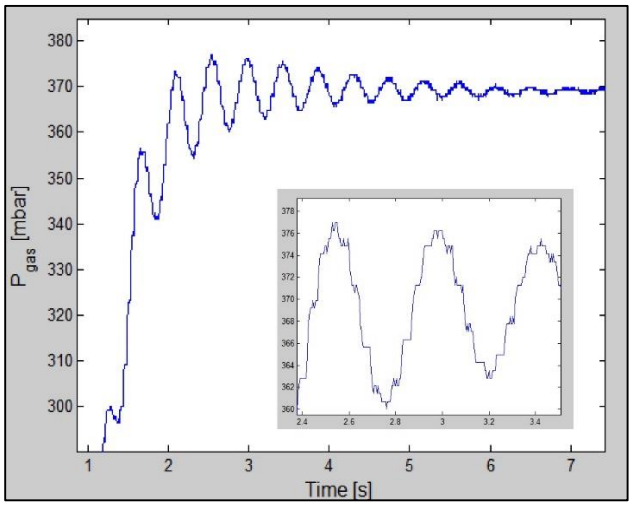

Figure 29: 10g/l CMC experiment: Pressure oscillations of gas with time.

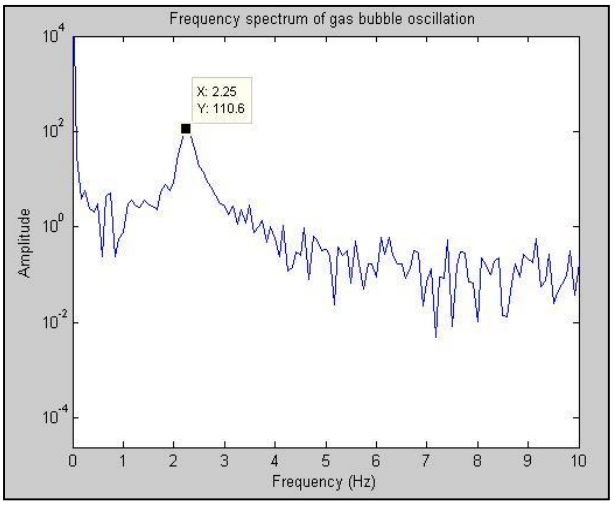

Figure 30: FFT Analysis, converting time into frequency.

As the 8cm i.id valve is opened, initiating the experiment, the initial pressure of 0mbar (gauge) rises to its maximum of 377mbar after 2.5 seconds. As the oscillation subsides, equilibrium is reached after roughly 7 seconds. The equilibrium pressure is 368mbar.

From the FFT Analysis in Fig.30, the predominant frequency is shown to be 2.25 Hz. This is then lower than the other fluids at 2.33 Hz, which is to be expected. Viscosity will affect the number of oscillation cycles per unit of time. As seen in the rheological experiments, the 10 g/l CMC is a more viscous fluid, even at the higher shear-rates (infinite-shear).

From the video images in Fig.31 it is clearly visible that this CMC concentration is more resistant towards compared to water.

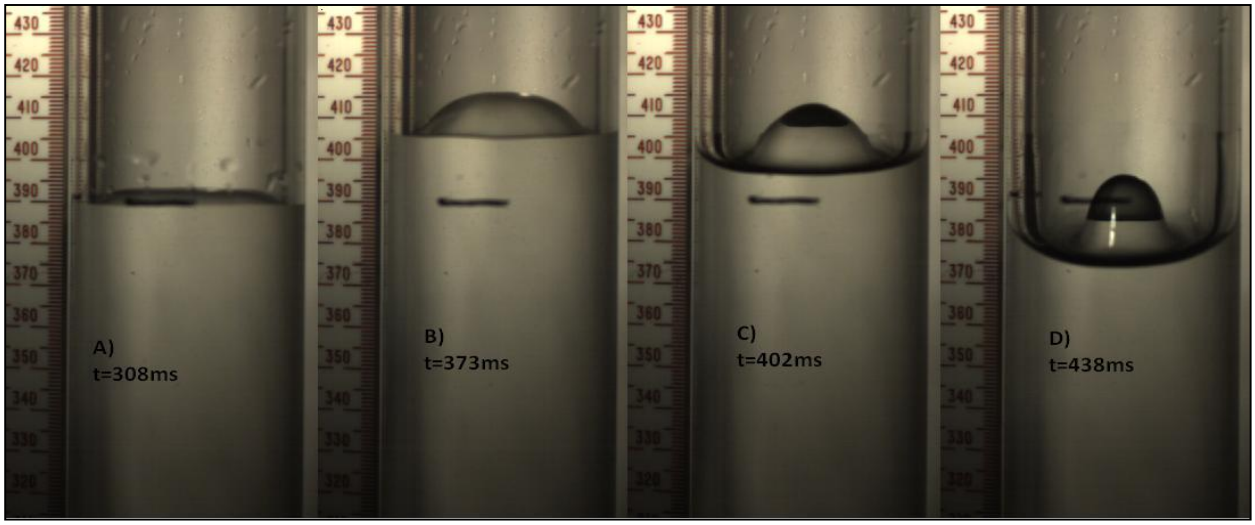

Figure 31: Depicts the first oscillation cycle of the 10g/l CMC experiment.

A - 308ms) Interface as it passes the equilibrium line upwards.
B - 373ms) As the interface comes to rest, the core continues to rise.
C - 402ms) The liquid core reaches its maximum point and starts to decend.
D - 438ms) The distance between the interior core and the exterior wall increases further. The interface now crosses the equilibrium line, draining downwards.

The maximum level of level of the interface, in this case, only reaches 25mm above the equilibrium line, all due to viscosity. The system still shows the properties described by Uchida[4].

4.3.1.5 PIV Analysis

Particle Image Velocimetry (PIV) was also used to complement the pressure- and video recordings. Copolymide tracer particles ("Griltex", *delivered by EMS-Chemie AG*) were added to the liquid in order to visualize the movement of the flow, thus revealing its velocity profile. An open source Matlab program (MatPIV, Sveen[16]) was utilized to perform two-dimentional cross correlation of the particle movement between two images taken at short intervals (Δt = 2ms). In Fig.32 is shown frame 799 with the calculated velocity profile inserted. The frame time is 1596 ms. This is 1126ms after start, and corresponds to the third oscillation cycle, similar to those seen in the figure above. The PIV images (8800 total) are recorded with image centre at the initial interface position, where the two valves are closed and the gas bubble is as standard conditions. This level is 13 cm below the equilibrium level. Thus the PIV analysis captures flow details slightly below the interface during the oscillations. From the analysis, the fluid velocity is determined to be between 1-2ms, which might be enough to put the flow in a turbulent state.

PIV analysis was only applied in the water experiments, but due to the similarity of the experiments, it is safe to assume that the same results would be found in both the CMC experiments as well. The goal for the PIV analysis is to obtain the velocity-profile, which is important with regards to the friction found in the system.

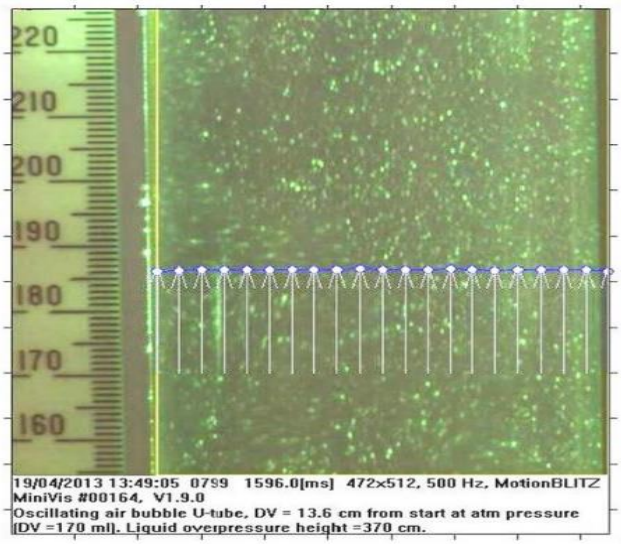

Figure 32: Velocity profile acquired through PIV. Water experiment

4.3.2 Pure U-Tube Oscillations

In order to get a better understanding of the flow friction in the rig, another experiment was conducted. This experiment differs from the previous one in the respect that this one omits the gas bubble. The gas bubble causes a lot of complexity when the flow behavior is to be simulated, and by omitting it, uncertainties like gas compressibility are circumvented.
The principle for this experiment is to drain 100ml liquid from the left pipe, and to add it to the right pipe. This creates a height difference (of 200ml) between the hydrostatic columns. When the right valve is opened, the system will start to flow and eventually reach equilibrium through energy dissipation in the form of friction.

The pure U-tube oscillation experiments contains test on water and 10g/l CMC. They were both executed in the same manner, as described below.

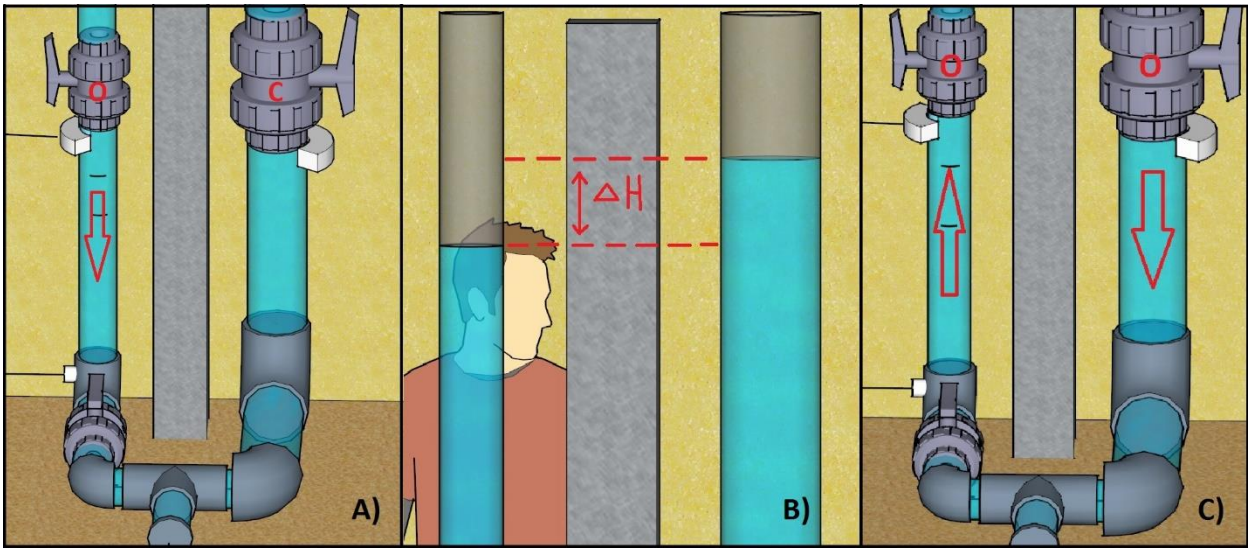

Figure 33: Shows the three steps of the Pure U-tube setup. Made in Google Sketchup by Kim Flatråker.

A) The right valve is closed while the left valve is kept open. 100 ml fluid is extracted through the drainage hose at the bottom of the rig. This will cause the level in the left pipe to drop 8cm.

B) The drained fluid is then poured back into the system in the right pipe, increasing the height difference further. There is now a 200 ml difference between the left and right pipe.

C) The right valve is opened, ensuring communication in the whole system. The fluid is set in an oscillatory motion where friction loss is the main parameter causing the system to reach equilibrium.

4.3.2.1 Pure U-tube Oscillations with Water

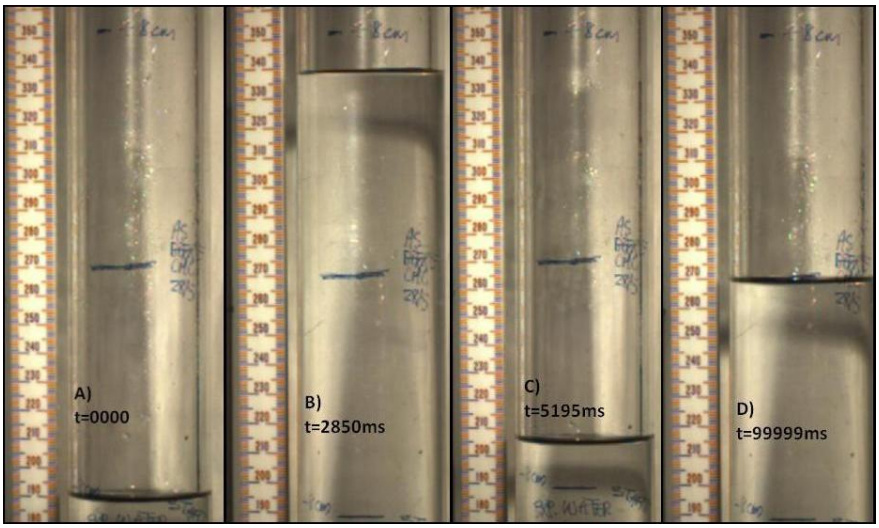

Figure 34: Shows the oscillation cycles of water in the pure U-tube.

Video images from the pure U-tube experiment are provided in Fig.34. The camera is directed at the left pipe, and only captures the oscillatory flow of the left liquid column. Do remember that the flow alternates up and down between the left and right pipe respectively. Three reference lines are drawn on the pipe. The middle one is the equilibrium line, whereas the line below shows the drained volume of 100ml which reduces the level by 8cm. The same line was also added 8cm above the equilibrium line. In a perfectly harmonic system, without any friction loss, the liquid level would have reached this line and would continue oscillating between these 8-cm lines indefinitely.

A) The liquid level at the start of the experiment. 8 cm below the equilibrium line.

B) 2.85seconds after the valve is opened, the liquid level reaches its maximum. Continuous piston-like fluid displacement.

C) The first oscillation cycle comes to an end after 5.2seconds. Notice that the liquid does not reach the 8cm line.

D) The system uses a long time in order to reach equilibrium. After 1min and 40seconds, small fluctuations are still visible on the interface.

In order to get a more accurate measurement of the pressure fluctuations in the flow rig during the U-tube oscillations, a third pressure sensor was installed. It is shown in Fig.35, and records the differential pressure between the valve and the bottom.

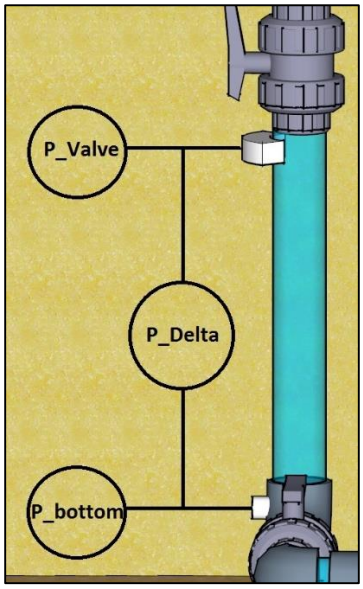

Figure 35: Shows the installation of the pressure sensor which records the pressure difference between the pressure at the valve and at the bottom. Created by Kim Flatråker using Google Sketchup.

An Interfase detection algorithm was written by Rune Time in Matlab. The algoritm uses a pixel intensity contrast in order to determine the location of the interfase from the video images. 10,000 images were analyzed and the variation in interfase height was plotted, as shown in Fig.36.

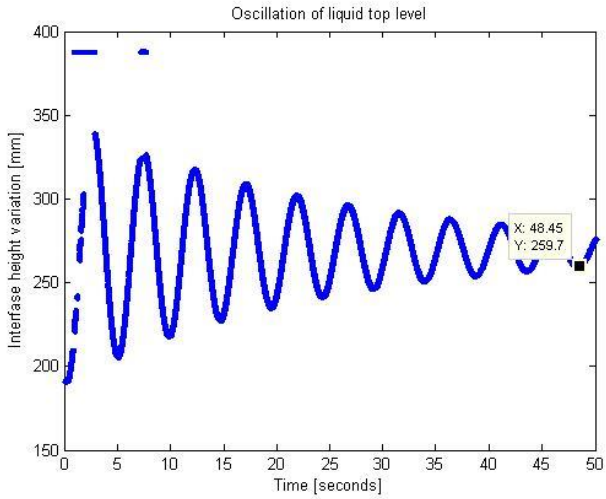

Figure 36: Shows the variation in interfase height vs. time.

From the plot, there are 10 oscillation periods after 48.45seconds have elapsed. This equals a frequency of 0.206Hz.This height plot is further complimented by the pressure sensors, which plot the variation in hydrostatic pressure. An FFT analysis was performed, and the dominant frequency was 0.208Hz, which coincides with the frequency found in the interface height variation plot.

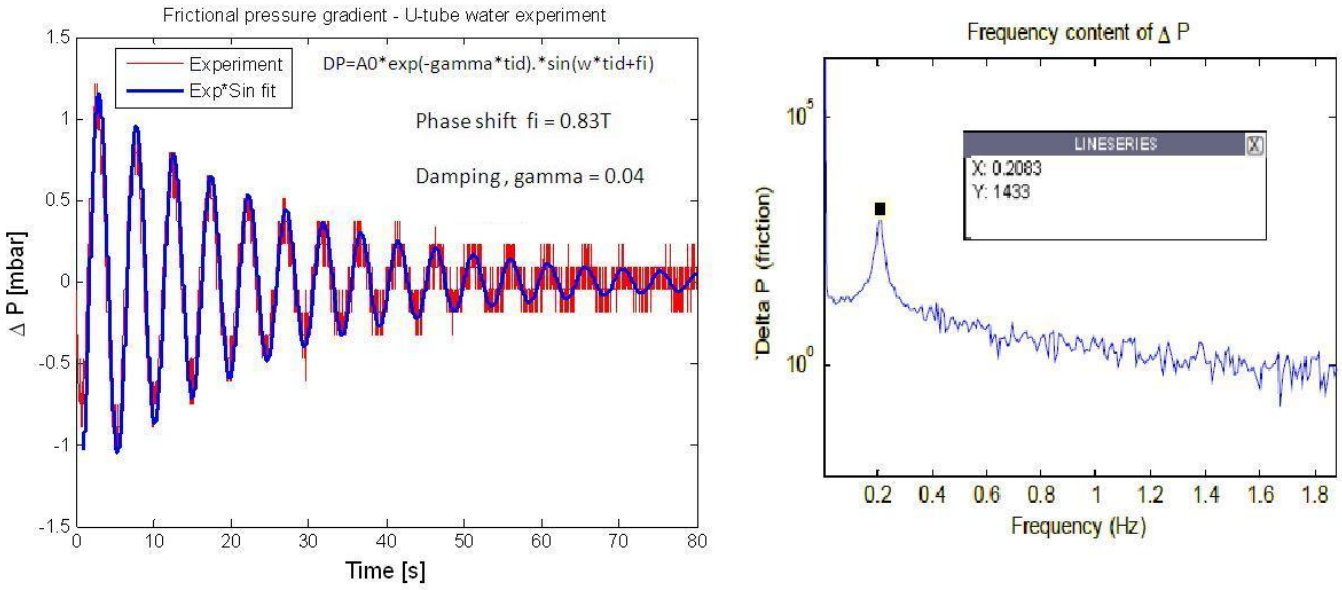

Figure 37: Shows the pressure variation with time. It also shows the frequency obtained through an FFT analysis.

In Fig.37, a curve-fit was applied to the pressure measurements. This yields information on the frictional pressure gradient ΔP, which is important for the numerical simulator, but will not be discussed in further detail here.

4.3.2.2 Pure U-tube Oscillations with 10g/l CMC

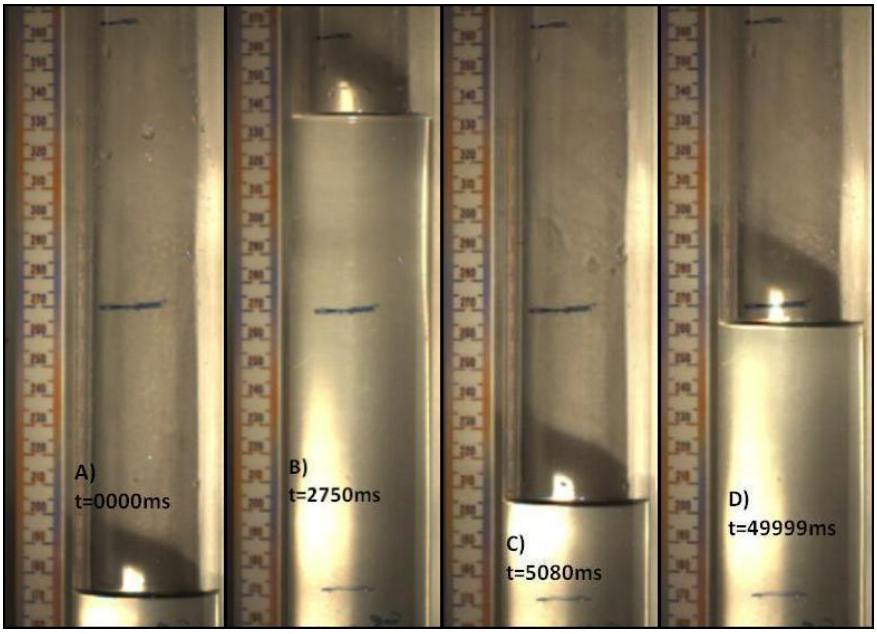

Figure 38: Shows the oscillation cycle of 10g/l CMC in the pure U-tube.

Video images from the pure U-tube with 10g/l CMC experiment are provided in Fig.38. Reference lines are also added to this experiment, although a close inspection reveals that they are 9.5cm above and below the equilibrium line. This is actually due to an error that occurred when the left pipe was being drained of 100ml. Some of the volume got "trapped" in the drainage hose, resulting in more liquid drained.

A) The liquid level at the start of the experiment.

B) The maximum liquid level is reached after 2.75seconds after the experiment is initiated. The CMC also exhibits continuous piston-like displacement.

C) The minimum level is reached after 5 seconds.

D) After 50 seconds the equilibrium is almost reached, although some movement is still visible. Notice that the level does not stop at the designated line, but almost a centimeter below. This is because a bit more than 100 ml was extracted from the system. One centimeter equals 12ml.

The same interface detection algorithm was applied to the 10g/l CMC experiment. The variation of the interface height is shown in Fig.39.

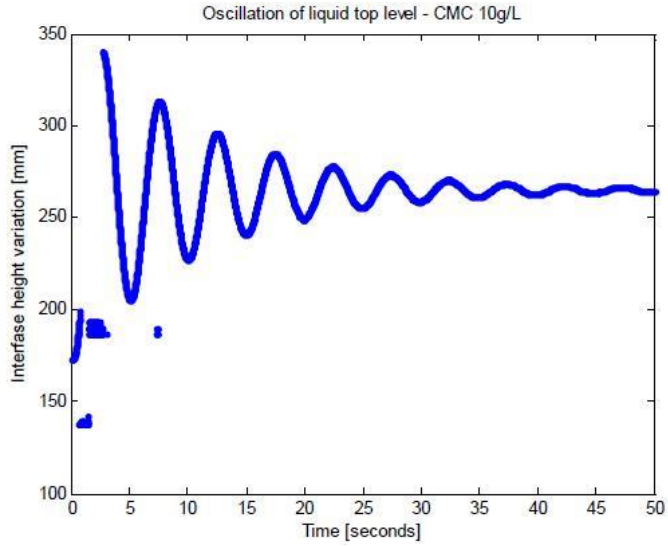

Figure 39: Shows the height of the interface varying with time.

During the initial 25 seconds of the experiment, 5 periods are visible in Fig 39. This equals a frequency of 0.200Hz. This coincides with the images shown in Fig.38, where the first oscillation cycle ended after 5 seconds.
The delta-pressure sensor was unfortunately not present at the 10g/l experiment. From the water experiments, however, the delta-pressure sensor gave the same results as found by the interface detection algorithm. There is therefore no reason to suspect that anything would be different in the case of 10g/l CMC had the sensor been available.

Note that the frequencies for both experiments are similar. The only difference is the viscous damping, which is much greater in the case of the CMC. This shows, once again, that when the viscosity is altered in any way, it will have a huge impact on the damping of the system.

5. MATHEMATICAL NUMERICAL SIMULATOR

After the experimental work, a numerical simulator of the flow rig was to be made using Matlab. This proved to be quite the task. With little-to-no training or experience with this software, several weeks went by with little progress and no results. Professor Rune Time[18] agreed that he would provide a helping hand. The following is taken from his paper on the subject.

In order to compare the experiments with theory beyond the analytical solutions in the (4) and (5) it was necessary to write a numerical simulator to include some of the many parameters which influences the behavior of the flow. A Matlab program was written to include geometry of the flow facility as well as the time-varying liquid level. It includes the gas-pocket compression and fluid friction. The program is simulating a set of time-dependent second order nonlinear equations.
It is based on a version of Newton's second law and mass conservation for gas and liquid. Written in a highly symbolic way, it is analogous to the undriven damped oscillator with the equation of motion;

$$m\ddot{x} + c\dot{x} + mgx + kx = 0 \qquad (9)$$

Where *m* is the liquid mass, *x* is displacement. The gas compression is described by using *k* as an elasticity-constant, *c* is connected to liquid viscosity.

- $m\ddot{x}$ is connected to Acceleration
- $c\dot{x}$ is connected to Viscous damping
- mgx is connected to Hydrostatic pressure / head
- kx is connected to Gas compressibility (Does not apply for the Pure U-tube)

The simulator includes the geometrical features of each section, the fluid properties and friction calculations. The compression of the gas bubble follows the equation of state for air, and has an option for simulating both isothermal and adiabatic compression.
There is no periodic external driving force except for the time-varying hydrostatic pressure difference. The acceleration is connected to the fraction of total mass in the two parts with different pipe diameters. The damping factor is wall friction together with so-called "singular pressure drops" in bends, expansions and valves. The solution procedure is to split the movement from start to end into small time-steps (1ms intervals) and solve for kinematics and dynamics.
Initially the acceleration is calculated. This is essentially bases on the net hydrostatic driving force, minus the friction forces. The net hydrostatic force is derived from the liquid level differences. Acceleration is calculated by dividing the sum of forces by the liquid mass. The acceleration and velocity in the two parts with different diameters are different, but are linked by the continuity equation. The speed and acceleration in the small left pipe is four times greater than in the right large pipe, since the diameter ratio equals two. After the acceleration has been found, the velocity is calculated based on the velocity at the previous time-step. Finally the position of the interfaces is updated based on the position at the previous time-step with the additional movement due to velocity and acceleration in the new time-step. All calculations are thus done in accordance with standard classical kinematics. Provided the time-steps are small enough the error in assuming constant acceleration is small.

Since the time-steps were so small, no special integration technique was needed, like e.g. Runge-Kutta or similar. In Fig.40, the simulated results from the flow experiment with water and a gas bubble are shown.

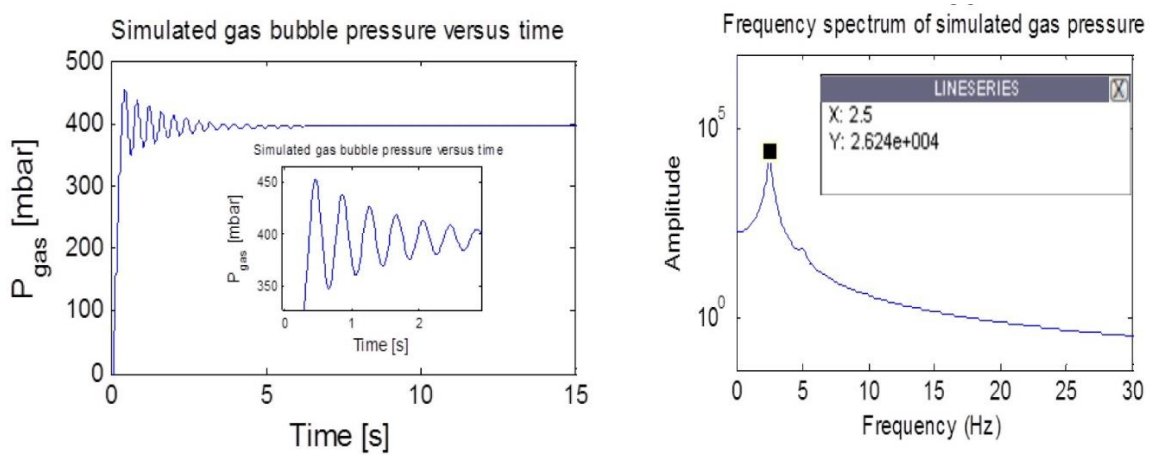

Figure 40: Numerical simulator of bubble pressure vs. time. The FFT analysis predicts a higher oscillation frequency than what is found in the experiments.

The simulator gives an oscillation frequency of 2.50Hz, which is higher than the 2.33Hz found from the experiments.

In Fig.41, the simulated results from the pure U-tube experiments are shown.

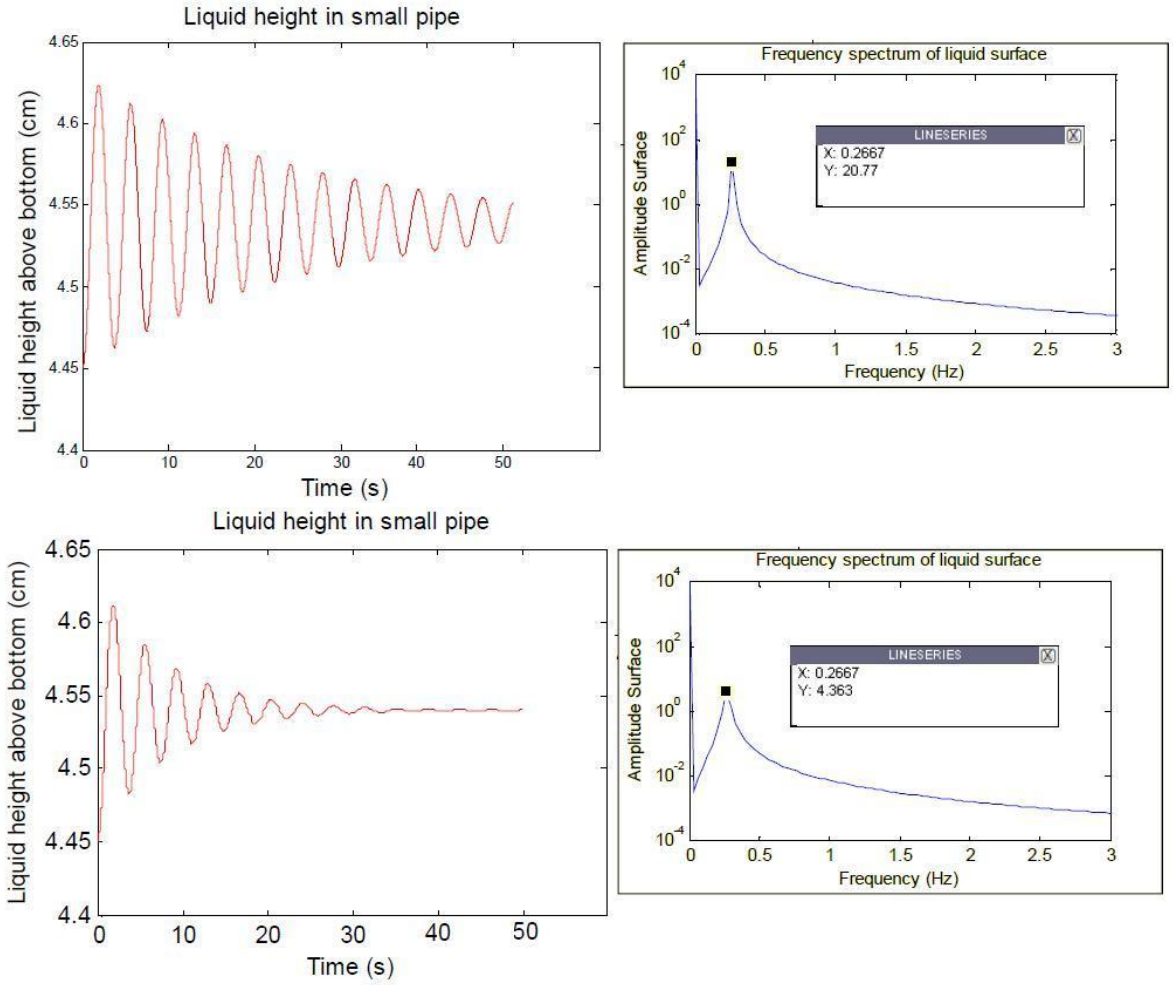

Figure 41: shows the simulated results from water and CMC respectively. Their FFT analysis is also given.

The oscillation frequency given by the simulator is 0.2667Hz in both cases, which are higher than the 0.210Hz found from the experiments.

The numerical simulations seem to overestimate the oscillation frequency slightly, at the same time as the initial damping is too low. For the classical damped harmonic oscillator it is well known that the friction term also impacts the oscillation frequency. The friction has been calculated using the standard pipe flow formulas for steady laminar and turbulent flow. However, all the experiments show similar results, that the frictional damping is much higher than predicted by simulation. In fact, during the initial transient, the turbulent friction factor in the simulations for the first two seconds had to be multiplied by a factor of 15 in order to dampen the initial oscillation of the to a level which was comparable to the gas kick experiments. However, there have been discussions, as in Manero et al[17], that oscillatory motion of non-Newtonian fluids might increase the flow-rate for certain pressure gradients. Time[18].

6. RESULTS - DISCUSSION

In the case of the experiment with a gas bubble in the flow rig, it is observed that when the valve is suddenly opened, the liquid will rise in the small pipe with a plug-like flow profile. As the interface passes the equilibrium level, the pressure is similar in both pipes. There is therefore no net driving pressure or pressure gradient in this situation. However, as the liquid rises and the pressure gradient plummets, the flow profile will change. The flow closest to the pipe wall will start to reverse and drain back downwards. Mass inertia causes a delay where the fluid closest to the wall drains whereas the liquid center / core remains static, with zero velocity profile. This is visible in the video images. The static core was coined a "Stalagmite" by Time et al[18]. The physics behind this phenomenon is somewhat similar to a pendulum in motion. When a pendulum is at its lowest point (closest to the ground) its velocity is at a maximum. When it reaches a horizontal position, its velocity is zero. All this at the expense of the potential energy associated with the movement, high potential energy equals low kinetic energy, and low potential energy equals high kinetic energy. In the flow rig, the velocity is closely related to the pressure gradient in the same manner. The oscillation found in the pipes seems to coincide with the discoveries made by Uchida[4].

The most noticeable difference between the entrapped gas experiment and the pure U-tube experiment is the damping. The frequency of U-tube oscillations with an entrapped gas pocket was more than 10 times higher than for the pure U-tube oscillations.

From the PIV analysis, the velocity of the fluid is found to be between 1-2 m/s. This is quite high and may well put the system in to a turbulent state. With turbulence, the steady-state model used by the simulator is well out of its boundary and does not handle the complexity this entails.
When it comes to the numerical simulator, it is observed that it is not able to correctly describe the damping found in the experiments, despite being mathematically sustainable. Thus it is concluded that for oscillatory flow, the normal way of calculating pressure drop may not be suitable for unsteady flows. The numerical model is based on a steady state flow, and this should hold true on both Newtonian and non-Newtonian fluids with or without the gas bubble. A solution to this predicament may be to discard the steady-state model and opt to calculate the friction factors and pressure drops using a more comprehensive models such as those described in Metzners et al[19] or Pilehvari et al[20]. The use of these advanced models however, may cause even more uncertainties in the form of unknown parameters.

The rheological experiments show that the CMC is a viscoelastic liquid. It does not exhibit any strong gelling properties, and the dominating attribute is the viscous one. It is uncertain if the simulator is able to properly model the viscoelastic properties of the fluid.

Observing the high speed video, it is clearly visible that the moving liquid is not radial symmetric. This is also supplemented by the PIV measurements. This is geometrically induced by the complexity in the U-tube. The bends and the crossover will cause the flow to move more quickly in the outer side of the turn within the bends. This distorts the flow profile and causes asymmetry, affect the friction and enhance shear stress. In the crossover the diameter is changed from an inner diameter of 8cm down to 4cm. This change in diameter will cause the liquid to accelerate and lose some of its pressure (as seen in a Venturi

nozzle). It is unknown how much this affects the overall system, but a closer investigation with the use of PIV would be interesting.

Overall, the comparison between experiments and the numerical model was shown to be more complicated than initially predicted or anticipated. The use of only hydrostatic pressure and friction is not enough to describe the observations made during the experiments.

7. CONCLUSION

The purpose of this thesis was to study rheological parameters as they are transferred from a small scale lab-test into a large scale drilling scenario. This was achieved by constructing a medium scale U-tube flow rig and studying oscillatory motion of different fluids. The experiments were conducted with the intentions of addressing uncertainties in this system. Parameters for both Newtonian and non-Newtonian liquids were investigated.
The complexity of the system and all the uncertain- and often unknown parameters- combined makes the simulation task very difficult. Parameters like flow-dynamics, heat dissipation in the gas-bubble, friction factors, pipe geometry, particles ("cuttings") and compressibility and viscoelasticity of the fluid have great impact on the rheology. Even though the rheological properties of a fluid are accurately determined, the overall flow dynamics and friction aspects of a complex system are hard to simulate. The effect of rheological parameters on the flow behavior is not straightforward. The experiments show that the most significant effect of fluid rheology in oscillations is on the damping.

This thesis is a part of a greater project here in the lab, and may well have triggered more questions than it answers. For example; why is the damping effect greater in the system than theory would predict? What is the actual friction factor and pressure loss in the bends and at the crossover? To get a better understanding of pressure loss and flow behavior in the flow rig, future work could be to divide the system into smaller segments and to study these segments separately with the use of PIV and pressure sensors.

8. REFERENCES

1. A.Saasen,G.Løkingholm: ”The Effect of Drilling Fluid Rheological Properties on Hole Cleaning”, *IADC/SPE 74558,* Dallas, Texas, 26-28 February 2002.

2. Schlicting: “Boundary Layer Theory”, McGraw-Hill, 1968, ISNB 07-055329-7.

3. J. N. Libii: “A Method of Evaluating the Presence of Fan-Blade-Rotation Induced Unsteadiness in Wind Tunnel Experiments” *Wind Tunnel Design and Their Diverse Engineering Applications,* Dr. Noor Ahmed (Ed.), ISBN: 978-953-51-1047-7, 2013, InTech, DOI: 10.5772/54144.
   http://www.intechopen.com/books/wind-tunnel-designs-and-their-diverse-engineering-applications/a-method-of-evaluating-the-presence-of-fan-blade-rotation-induced-unsteadiness-in-wind-tunnel-experi

4. S. Uchida: “The Pulsating Viscous Flow Superposed on the Steady Laminar Motion of Incompressible Fluid in a Circular Pipe”, *ZAMP 7, pp* 403-411 .1956.

5. Thomas G. Mezger: “The Rheology Handbook: For Users of Rotational and Oscillatory Rheometers” 3rd Revised Edition,Hannover; Vincentz Network, Coatings Compendia, 2006, ISBN 3-87870-174-8

6. Fast Fourier Transform
   http://en.wikipedia.org/wiki/Fast_fourier
   Visited 4/6-2013

7. Dantec Dynamics, Laser Optical Measurement Systems and Sensors.
   http://www.dantecdynamics.com/Default.aspx?ID=1049
   Visited 5/6-2013

8. L. Cisneros, Post Doc. Associate “Collective Dynamics in Suspensions of Concentrated Swimming Micro-Organisms” http://www.physics.arizona.edu/~cisneros/publications.html
   Visited 5/6-2013

9. Differential Capacitance Pressure Sensors
   http://instrumenttoolbox.blogspot.no/2011/02/electrical-pressure-sensors-used-in_13.html
   Visited 6/5-2013

10. The Rosemound 3051 Pressure Transmitter;
    http://www2.emersonprocess.com/en-us/brands/rosemount/pressure/pressure-transmitters/3051-pressure-transmitters/pages/index.aspx
    Visited 6/5-2013

11. Anton Paar MCR 302 Series Instruction Manual, Software version 3.62. 2011. Anton Paar GmbH, Graz, AustriaDocument Number: C92IB001EN-C

12. P. K. Kennedy: "*Flow Analysis of Injection Molds*", Hanser-Gardner Publications 1995, ISBN 1-56990-181-3

13. Anton Paar DMA 4500/5000 Densiry/Specific Gravity/Concentration Meter, Software Version:v2.004.g, Instruction Handbook. 1998. Anton Paar GmbH, Graz, Austria Document Number: xdlib07c.pm5

14. H. M. Park: "Rheometry Using Velocity Measurements", *Rheologica Acta,* 2009, 48:433-445.

15. A. Ogawa: "Damping Vibrational Motion of Liquid Column in Vertical U-Tube for Newtonian and non-Newtonian Liquids" *Proceedings of the 8th International Symposium on Experimental and Computational Aerothermodynamics of Internal Flows,* Lyon, July 2007, Paper ref: ISAIF8-009 http://www.lmfa.ec-lyon.fr/ISAIF/Data/Papers/44_07-01-11_ISAIF8-009_Ogawa.pdf

16. Sveen, J.K.: "MatPIV", Department of Mathematics, University of Oslo, 2004.

17. O. Manero, B. Mena: "An Interesting Effect in non-Newtonian Flow in Oscillating Pipes", *Rheologica Acta,* Fall 1977, Volume 16, Issue 5, pp 573-576; http://link.springer.com/article/10.1007%2FBF01525658#

18. R. W. Time, A. H. Rabenjafimanantsoa: "On the Relevance of Laboratory Scale Rheometric Measurements for Calculation of Complex Large Scale Flows in Well Drilling and Pipe Flows" *Annual Transactions of the Nordic Rheology Society* Volume 22, 2013

19. A. B. Metzner, J.C Reed: "Flow of non-Newtonian Fluid-Correlation of the Laminar, Transition and Turbulent Flow Regions", *AIChe Journal,* pp 434-440, 1955

20. A. Pilehvari, R. Perth: "Generalized Hydraulic Calculation Method for Axial Flow of non-Newtonian Fluid in Eccentric Annuli", December 2009, *SPE Drilling and Completion,* pp 553-563.

9. APPENDIX

The following is only excerpts of the allocated files provided on the CD of this thesis. The sheer size of the data files are simply too great to be presented in the form of tables.

```
% Simulate dynamic oscillation in experimental U-tube
clc
clear all
format compact
g=9.81    % Tyngdeakselerasjon
P0=1e5    % Atmosfæretrykk
rol=1000 % Væsketetthet
myl=1e-3 % Væskeviskositet

% Two vertical risers with inner diameters D1 and D2. Connected via a bend
% system with adapter from D1 to D2

D1=0.08 % Biggest riser pipe
D2=0.04
A1=pi*D1^2/4
A2=pi*D2^2/4

HV2=1.5 % Høyde opp til ventil i 4 cm røret
H1init=4   %initiell væskehøyde - stengt ventil i det store røret
H2init=1.47 %initiell væskehøyde i det tynne røret

%Volumkonservering
HTOT=H1init*A1+H2init*A2

PGgaugeinit=0.3e5% Initielt fritt valgt gassbobletrykk
farge='-r' % Brukes i plottene i figur 1
farge='-b'
farge='-g'

% PGgaugeinit=(H1init-H2init)*rol*g %skal gi null endring i væske nivå -
% virker OK!
PGinit=P0+PGgaugeinit
% Initielt boblevolum
VGinit=(HV2-H2init)*A2

% Ideal gass (rog = rogref *PG/Pref, Pref = 1 bar)
rogref = 1.2
Pref=1e5
roginit=rogref*PGinit/Pref

% Gass masse
MG = VGinit*roginit

```

Appendix 1: Excerpt from the Numerical Simulator part 1.

```
44
45      % ************ ANALYTISKE LØSNINGER START ***********************
46      % 1) Beregn likevekts høyder (se powerpoint analyse):
47 -    A=(A1/A2)-1
48
49 -    K1=HV2-H2init
50 -    K2=H1init-H2init
51 -    B=-(PO/(rol*g)+K2+A*K1)
52 -    C=-(PGgaugeinit/(rol*g)-K2)*K1
53
54 -    DH21=(-B+sqrt(B^2-4*A*C))/(2*A) % Ikkefysisk rot
55 -    DH22=(-B-sqrt(B^2-4*A*C))/(2*A)
56 -    H2O=H2init+DH22
57 -    H1O=H1init-DH22*A2/A1
58
59       % 2)  Naiv beregning - hvor mye må gassbobla komprimeres for det opprinnelige
60       %overtrykket
61 -     Overtrykk=rol*g*(H1init-H2init)
62 -     VGny=VGinit*PGinit/(PO+Overtrykk)
63 -     DiffH2=(VGinit-VGny)/A2
64 -     H2NY=H2init+DiffH2
65
66      % 3) NY ANALYTISK LØSNING - papir side 10
67 -    alfa=PGinit*(HV2-H2init)
68 -    AR=A2/A1-1
69 -    F=AR*rol*g
70 -    beta=alfa-PO*HV2
71 -    BB=HV2-PO/F
72 -    CC=beta/F
73 -    H2O1=(BB+sqrt(BB^2-4*C))/2
74 -    H2O2=(BB-sqrt(BB^2-4*C))/2
75
76      % 4) ENDA EN ANALYTISK side 11 i papirutgaven
77 -    ARP=A2/A1+1
78 -    AAA=ARP*rol*g
79 -    gamma=H1init+H2init*A2/A1
80 -    BBB=AAA*HV2+gamma*rol*g+PO
81 -    CCC=gamma*rol*g*HV2-beta
82 -    H2O1m=(BBB+sqrt(BBB^2-4*AAA*CCC))/(2*AAA) % Ufysikalsk
83 -    H2O2m=(BBB-sqrt(BBB^2-4*AAA*CCC))/(2*AAA) % Denne er riktig
84 -    H1O2m = H1init- (H2O2m-H2init)*A2/A1 % Beregner tilsvarende H1 nivå
85
```

Appendix 2: Excerpt from the Numerical Simulator part 2.

```
1
2       % ************************************
3       % Postprosessering av data
4       % ************************************
5 -     clc
6 -     clf
7
8 -     Filnavn = 'Free U-Tube 10gpl CMC 28 mai Run4.xls';
9
10 -    newcalc=1
11 -    if newcalc ==1
12      %clear all
13 -    [Xldata, Xltekst] = xlsread(Filnavn);
14 -    end
15
16
17 -    Trykk_flow = Xldata;
18
19 -    d = 0.04;
20 -    A = pi().*d^2/4;
21
22
23 -    time = Trykk_flow(:,1);
24 -    P_bunn = Trykk_flow(:,2);
25 -    P_ventil = Trykk_flow(:,3);
26 -    P_diff=Trykk_flow(:,4);
27
28 -    figure(1);
29 -    Start = 1
30 -    Stopp = 20000;
31 -    plot(time,P_ventil,'-b');
32 -    xlabel('Time [s]','Fontsize',12);
33      % ylabel('P_{0} [mbar]','Fontsize',12);
34 -    ylabel('P_{valve} [mbar]','Fontsize',12);
35
36
37 -    figure(2);
38 -    plot(time,P_bunn,'-b');
39 -    xlabel('Time [s]','Fontsize',12);
40 -    ylabel('P_bottom [mbar]','Fontsize',12);
41      %ymin = 300; ymax = 350;
42      %axis([3 13 ymin ymax]);
43
44 -    figure(3)
45 -    plot(P_bunn,P_ventil,'-k');
46 -    xlabel('P_bunn [mbar]','Fontsize',12);
47 -    ylabel('P_{0} [mbar]','Fontsize',12);
48      %ymin = 300; ymax = 350;
49      %axis([3 13 ymin ymax]);
```

Appendix 3: Excerpt of the Post-processing code used to analyze the Excel Data. "oscillering"

	A	B	C	D	E	F	G	H
5481	21.92	329.314	330.388	0.095	0.063	0.015	0.015	0.02
5482	21.924	329.314	329.682	0.095	0.063	0.015	0.015	0.015
5483	21.928	328.612	329.682	0.095	0.063	0.015	0.015	0.015
5484	21.932	329.314	329.682	-0.045	-0.077	0.015	0.015	0.02
5485	21.936	329.314	330.388	0.095	-0.077	0.015	0.015	0.015
5486	21.94	329.314	329.682	0.095	0.063	0.015	0.02	0.015
5487	21.944	330.72	330.388	0.095	0.063	0.015	0.02	0.015
5488	21.948	328.612	330.388	-0.045	0.063	0.015	0.015	0.005
5489	21.952	330.72	329.682	0.095	0.063	0.015	0.015	0.015
5490	21.956	329.314	329.682	0.095	0.063	0.015	0.015	0.015
5491	21.96	329.314	330.388	0.095	0.063	0.015	0.015	0.015
5492	21.964	329.314	329.682	-0.045	0.063	0.015	0.015	0.015
5493	21.968	327.909	331.093	-0.045	-0.077	0.015	0.015	0.02
5494	21.972	328.612	329.682	0.095	0.063	0.015	0.005	0.015
5495	21.976	328.612	329.682	0.095	0.063	0.015	0.015	0.02
5496	21.98	329.314	329.682	0.095	0.063	0.015	0.02	0.015
5497	21.984	328.612	329.682	0.095	0.063	0	0.02	0.015
5498	21.988	330.017	329.682	0.095	0.063	0.015	0.015	0.015
5499	21.992	330.017	330.388	0.095	0.063	0.02	0.015	0.02
5500	21.996	327.909	330.388	0.095	0.063	0.015	0.02	0.015
5501	22	329.314	330.388	0.095	0.063	0.015	0.015	0.015
5502	22.004	328.612	330.388	0.095	0.063	0.015	0.02	0.015
5503	22.008	328.612	330.388	0.095	-0.077	0.015	0.02	0.015
5504	22.012	329.314	330.388	0.095	0.063	0.015	0.02	0.02
5505	22.016	329.314	330.388	0.095	0.063	0.015	0.015	0.015
5506	22.02	328.612	330.388	0.095	0.063	0.015	0.015	0.02
5507	22.024	330.017	329.682	-0.045	0.063	0.02	0.015	0.015
5508	22.028	329.314	330.388	0.095	0.063	0.015	0.015	0.015
5509	22.032	330.017	329.682	0.095	0.063	0.015	0.015	0.015
5510	22.036	330.017	329.682	0.095	0.063	0.015	0.015	0.015
5511	22.04	327.909	330.388	-0.045	0.063	0.015	0.015	0.015
5512	22.044	328.612	330.388	0.095	0.063	0.015	0.015	0.015
5513	22.048	328.612	330.388	-0.045	0.063	0.015	0.02	0.015
5514	22.052	329.314	329.682	-0.045	-0.077	0.015	0.02	0.015
5515	22.056	329.314	330.388	0.095	-0.077	0.015	0.015	0.015
5516	22.06	329.314	329.682	0.095	0.063	0.015	0.015	0.02
5517	22.064	327.909	330.388	0.095	0.063	0.02	0.015	0.02
5518	22.068	329.314	329.682	0.095	0.063	0.015	0.015	0.02
5519	22.072	330.017	330.388	0.095	0.063	0.015	0.015	0.015
5520	22.076	327.909	330.388	0.095	-0.077	0.015	0.015	0.015
5521	22.08	329.314	330.388	0.095	0.063	0.015	0.02	0.015
5522	22.084	330.017	330.388	0.095	0.063	0.015	0.015	0.015
5523	22.088	328.612	330.388	-0.045	0.063	0.015	0.015	0.015
5524	22.092	330.72	329.682	0.095	-0.077	0.015	0.02	0.02
5525	22.096	329.314	330.388	0.095	-0.077	0.015	0.015	0.015
5526	22.1	329.314	329.682	0.095	0.063	0.015	0.015	0.015
5527	22.104	328.612	330.388	-0.045	0.063	0.02	0.02	0.015
5528	22.108	329.314	330.388	-0.045	0.063	0.015	0.015	0.015
5529	22.112	328.612	330.388	0.095	0.063	0.015	0.015	0.02
5530	22.116	328.612	329.682	0.095	0.063	0.015	0.015	0.015
5531	22.12	330.72	329.682	-0.045	-0.077	0.015	0.015	0.015
5532	22.124	328.612	329.682	0.095	0.063	0.015	0.015	0.015
5533	22.128	330.017	330.388	0.095	0.063	0.015	0.02	0.015
5534	22.132	329.314	330.388	-0.045	0.063	0.015	0.02	0.02
5535	22.136	329.314	329.682	0.095	0.063	0.015	0.015	0.02
5536	22.14	329.314	329.682	-0.045	0.063	0.015	0.015	0.02
5537	22.144	327.909	330.388	-0.045	-0.077	0.015	0.015	0.015
5538	22.148	329.314	329.682	-0.045	0.063	0.015	0.02	0.015
5539	22.152	329.314	330.388	0.095	0.063	0.015	0.015	0.015
5540	22.156	328.612	330.388	0.095	0.063	0.015	0.015	0.015
5541	22.16	328.612	329.682	-0.045	-0.077	0.015	0.02	0.015
5542	22.164	330.017	330.388	0.095	0.063	0.015	0.015	0.02
5543	22.168	329.314	330.388	0.095	0.063	0.015	0.015	0.015
5544	22.172	329.314	330.388	0.095	0.063	0.02	0.015	0.015
5545	22.176	329.314	329.682	0.095	0.063	0.015	0.015	0.015
5546	22.18	328.612	330.388	-0.045	0.063	0.015	0.015	0.015
5547	22.184	329.314	330.388	-0.045	-0.077	0.015	0.02	0.015
5548	22.188	329.314	329.682	0.095	0.063	0.015	0.02	0.015
5549	22.192	329.314	330.388	0.095	0.063	0.015	0.02	0.015
5550	22.196	328.612	329.682	0.095	0.063	0.015	0.015	0.015
5551								
5552	Time	P0	P_Bunn					

Appendix 4: Excerpt of the data from "Gas Kick experiment with Water."

	A	B	C	D	E	F	G	H
4947	19.784	330.72	360.01	-0.045	0.063	0.015	0.015	0.02
4948	19.788	332.125	360.01	-0.186	0.203	0.015	0.015	0.015
4949	19.792	331.422	359.305	-0.045	0.063	0.015	0.015	0.015
4950	19.796	330.72	360.01	-0.045	0.203	0.015	0.02	0.015
4951	19.8	331.422	360.01	-0.045	0.063	0.015	0.015	0.015
4952	19.804	331.422	359.305	-0.045	0.063	0.02	0.015	0.015
4953	19.808	330.72	359.305	-0.045	0.063	0.015	0.02	0.015
4954	19.812	332.125	359.305	-0.045	0.063	0.015	0.015	0.015
4955	19.816	331.422	360.01	-0.045	0.063	0.015	0.015	0.02
4956	19.82	331.422	360.01	-0.045	0.203	0.015	0.015	0.02
4957	19.824	331.422	359.305	-0.045	0.203	0.015	0.015	0.015
4958	19.828	330.72	359.305	-0.045	0.063	0.02	0.015	0.02
4959	19.832	330.72	360.01	-0.045	0.063	0.015	0.015	0.02
4960	19.836	330.017	360.01	-0.045	0.063	0.015	0.02	0.02
4961	19.84	330.72	360.01	-0.045	0.063	0.015	0.02	0.015
4962	19.844	331.422	360.01	-0.045	0.063	0.015	0.02	0.015
4963	19.848	330.017	359.305	0.095	0.063	0.015	0.015	0.02
4964	19.852	330.72	359.305	-0.045	0.063	0.015	0.015	0.015
4965	19.856	332.125	359.305	-0.045	0.063	0.015	0.015	0.02
4966	19.86	330.72	359.305	-0.186	0.063	0.015	0.02	0.015
4967	19.864	331.422	360.01	-0.186	0.063	0.02	0.015	0.015
4968	19.868	330.72	359.305	-0.045	0.203	0.02	0.02	0.015
4969	19.872	331.422	359.305	-0.045	0.063	0.015	0.015	0.02
4970	19.876	331.422	359.305	-0.045	0.063	0.015	0.015	0.02
4971	19.88	331.422	360.01	-0.045	0.063	0.015	0.02	0.015
4972	19.884	330.72	360.01	-0.045	0.063	0.015	0.015	0.015
4973	19.888	330.72	360.01	-0.045	0.063	0.015	0.015	0.015
4974	19.892	330.017	360.01	-0.045	0.063	0.015	0.015	0.015
4975	19.896	330.017	359.305	-0.045	0.063	0.015	0.015	0.02
4976	19.9	331.422	359.305	-0.045	0.063	0.015	0.015	0.015
4977	19.904	330.017	360.01	-0.045	0.063	0.015	0.02	0.015
4978	19.908	330.72	359.305	-0.045	0.063	0.015	0.015	0.015
4979	19.912	330.72	360.01	-0.045	0.063	0.015	0.015	0.02
4980	19.916	330.72	359.305	-0.045	0.063	0.015	0.015	0.02
4981	19.92	332.125	360.01	-0.045	0.063	0.015	0.015	0.015
4982	19.924	330.72	359.305	-0.045	0.203	0.02	0.02	0.02
4983	19.928	332.828	359.305	-0.045	0.063	0.015	0.015	0.015
4984	19.932	331.422	360.01	0.095	0.063	0.015	0.015	0.015
4985	19.936	331.422	360.01	-0.045	0.063	0.015	0.015	0.02
4986	19.94	331.422	359.305	-0.045	0.063	0.015	0.015	0.02
4987	19.944	330.72	360.01	-0.045	-0.077	0.02	0.02	0.02
4988	19.948	331.422	360.01	-0.186	0.063	0.015	0.015	0.02
4989	19.952	330.017	360.01	-0.045	0.063	0.02	0.015	0.02
4990	19.956	331.422	359.305	-0.045	0.063	0.02	0.02	0.02
4991	19.96	330.72	360.01	-0.045	0.063	0.015	0.015	0.015
4992	19.964	331.422	359.305	-0.045	0.203	0.015	0.015	0.015
4993	19.968	330.72	360.01	-0.045	0.063	0.015	0.015	0.015
4994	19.972	332.125	359.305	-0.045	0.063	0.015	0.015	0.02
4995	19.976	330.72	359.305	-0.045	0.063	0.015	0.015	0.015
4996	19.98	330.72	360.01	-0.045	0.203	0.015	0.015	0.015
4997	19.984	332.125	359.305	0.095	0.063	-0.005	0.015	0.02
4998	19.988	330.017	360.01	-0.045	0.063	0.015	0.02	0.015
4999	19.992	331.422	359.305	-0.045	0.063	0.015	0.015	0.015
5000	19.996	329.314	359.305	-0.045	0.063	0.015	0.02	0.015

Appendix 5: Excerpt of the data from "Gas Kick Experiment with 1g-l CMC."

	A	B	C	D	E	F	G	H
4894	19.572	334.233	367.769	2.201	-1.899	0.015	0.02	0.015
4895	19.576	333.531	367.769	2.201	-1.899	0.015	0.015	0.02
4896	19.58	334.936	367.769	2.201	-1.899	0.015	0.02	0.015
4897	19.584	334.233	368.474	2.201	-1.899	0.015	0.015	0.015
4898	19.588	335.639	367.769	2.201	-1.899	0.015	0.015	0.02
4899	19.592	334.233	368.474	2.201	-1.899	0.015	0.015	0.015
4900	19.596	334.233	368.474	2.201	-1.899	0.015	0.015	0.015
4901	19.6	334.233	368.474	2.201	-1.899	0.015	0.015	0.015
4902	19.604	334.936	367.769	2.201	-1.899	0.015	0.015	0.015
4903	19.608	334.233	368.474	2.201	-1.899	0.015	0.015	0.02
4904	19.612	334.936	368.474	2.201	-1.759	0.015	0.015	0.015
4905	19.616	335.639	367.769	2.201	-1.899	0.015	0.015	0.015
4906	19.62	335.639	368.474	2.201	-1.899	0.015	0.02	0.015
4907	19.624	335.639	368.474	2.201	-1.899	0.015	0.015	0.015
4908	19.628	334.936	368.474	2.201	-1.899	0.015	0.015	0.02
4909	19.632	334.936	368.474	2.201	-1.899	0.015	0.015	0.015
4910	19.636	334.936	368.474	2.201	-1.899	0.015	0.02	0.015
4911	19.64	334.936	367.769	2.201	-1.899	0.015	0.015	0.015
4912	19.644	334.936	368.474	2.201	-1.899	0.015	0.02	0.015
4913	19.648	334.936	368.474	2.201	-1.899	0.015	0.005	0.02
4914	19.652	334.233	369.18	2.201	-1.899	0.015	0.02	0.015
4915	19.656	334.936	368.474	2.201	-1.899	0.015	0.02	0.015
4916	19.66	333.531	368.474	2.201	-1.899	0.015	0.02	0.02
4917	19.664	334.936	367.769	2.201	-1.759	0.015	0.015	0.015
4918	19.668	334.233	368.474	2.342	-2.04	0.02	0.015	0.02
4919	19.672	334.936	368.474	2.201	-1.899	0.015	0.02	0.015
4920	19.676	334.936	368.474	2.201	-1.899	0.02	0.015	0.015
4921	19.68	334.936	368.474	2.342	-1.759	0.02	0.015	0.015
4922	19.684	334.936	368.474	2.201	-1.899	0.02	0.015	0.015
4923	19.688	333.531	368.474	2.201	-1.899	0.01	0.015	0.02
4924	19.692	334.233	367.769	2.201	-1.899	0.015	0.015	0.015
4925	19.696	333.531	367.769	2.201	-1.899	0.015	0.015	0.015
4926	19.7	334.233	368.474	2.201	-1.899	0.015	0.015	0.015
4927	19.704	334.233	367.769	2.201	-1.899	0.015	0.015	0.02
4928	19.708	334.233	367.769	2.061	-1.899	0.015	0.015	0.02
4929	19.712	334.233	368.474	2.201	-1.899	0.015	0.015	0.015
4930	19.716	334.233	367.769	2.201	-1.899	0.015	0.015	0.015
4931	19.72	333.531	367.769	2.201	-1.899	0.015	0.015	0.015
4932	19.724	334.936	367.769	2.201	-1.899	0.02	0.015	0.015
4933	19.728	334.936	368.474	2.201	-1.899	0.015	0.015	0.02
4934	19.732	335.639	368.474	2.201	-1.899	0.015	0.015	0.015
4935	19.736	334.233	367.769	2.201	-1.759	0.015	0.02	0.015
4936	19.74	335.639	368.474	2.201	-1.899	0.015	0.015	0.015
4937	19.744	334.233	367.769	2.201	-1.899	0.015	0.015	0.015
4938	19.748	334.936	367.769	2.201	-1.899	0.015	0.015	0.02
4939	19.752	334.233	368.474	2.201	-1.899	0.015	0.015	0.02
4940	19.756	333.531	367.769	2.201	-1.899	0.015	0.015	0.015
4941	19.76	334.936	367.769	2.201	-1.899	0.015	0.015	0.015
4942	19.764	334.233	368.474	2.201	-1.759	0.015	0.015	0.015
4943	19.768	336.342	367.769	2.201	-1.759	0.015	0.015	0.005
4944	19.772	334.233	367.769	2.201	-1.759	0.015	0.015	0.015
4945	19.776	334.936	368.474	2.201	-1.899	0.015	0.015	0.015
4946	19.78	334.233	368.474	2.201	-1.759	0.015	0.02	0.015
4947	19.784	334.936	368.474	2.342	-1.899	0.02	0.015	0.015
4948	19.788	333.531	368.474	2.201	-1.899	0.015	0.02	0.015
4949	19.792	334.936	367.769	2.201	-1.899	0.015	0.015	0.015
4950	19.796	334.936	368.474	2.201	-1.899	0.015	0.015	0.02

Appendix 6: Excerpt of the data from "Gas Kick Experiment with 10g-l CMC."

	A	B	C	D	E	F	G	H
30356	121.416	317.368	326.861	-0.045	0.063	0.015	0.015	0.02
30357	121.42	315.962	326.861	-0.045	-0.077	0.015	0.02	0.015
30358	121.424	315.962	326.861	-0.045	-0.077	0.015	0.015	0.02
30359	121.428	315.962	326.861	-0.045	-0.077	0.015	0.015	0.015
30360	121.432	315.259	326.156	-0.186	0.063	0.015	0.015	0.02
30361	121.436	316.665	326.861	-0.045	-0.077	0.015	0.015	0.02
30362	121.44	316.665	326.861	-0.045	0.063	0.015	0.015	0.02
30363	121.444	317.368	326.156	-0.045	0.063	0.02	0.02	0.015
30364	121.448	317.368	326.861	-0.045	0.063	0.015	0.015	0.02
30365	121.452	316.665	326.156	-0.045	-0.077	0.015	0.015	0.015
30366	121.456	317.368	326.156	0.095	0.063	0.015	0.02	0.02
30367	121.46	316.665	326.861	-0.045	0.063	0.015	0.015	0.015
30368	121.464	317.368	326.861	-0.045	-0.077	0.015	0.015	0.02
30369	121.468	315.962	326.861	-0.045	0.063	0.015	0.015	0.015
30370	121.472	316.665	326.861	0.095	0.063	0.015	0.02	0.02
30371	121.476	315.962	326.156	-0.045	0.063	0.015	0.015	0.015
30372	121.48	315.962	326.861	0.095	0.063	0.015	0.015	0.015
30373	121.484	317.368	326.861	-0.045	0.063	0.015	0.015	0.015
30374	121.488	315.962	326.156	-0.045	0.063	0.015	0.015	0
30375	121.492	317.368	326.861	-0.045	0.063	0.015	0.015	0.02
30376	121.496	316.665	326.861	-0.045	0.063	0.02	0.015	0.01
30377	121.5	317.368	326.861	-0.045	-0.077	0.015	0.015	0.015
30378	121.504	318.07	326.156	-0.045	0.063	0.015	0.015	0.015
30379	121.508	317.368	326.861	-0.045	0.063	0.015	0.015	0.015
30380	121.512	315.962	326.156	0.095	0.063	0.015	0.015	0.015
30381	121.516	315.962	326.861	-0.045	0.063	0.015	0.015	0.015
30382	121.52	316.665	326.861	-0.045	0.063	0.015	0.015	0.02
30383	121.524	316.665	326.861	-0.045	0.063	0.015	0.02	0.015
30384	121.528	318.07	326.861	-0.045	0.063	0.015	0.02	0.02
30385	121.532	316.665	326.156	0.095	0.063	0.015	0.015	0.015
30386	121.536	317.368	326.861	-0.045	0.063	0.015	0.015	0.02
30387	121.54	318.07	326.861	-0.045	0.063	0.015	0.015	0.015
30388	121.544	317.368	326.156	-0.045	0.063	0.015	0.015	0.02
30389	121.548	318.773	326.156	-0.045	0.063	0	0.015	0.015
30390	121.552	317.368	326.861	-0.045	0.063	0.015	0.015	0.015
30391	121.556	318.07	326.861	0.095	0.063	0.015	0.015	0.015
30392	121.56	317.368	326.861	-0.045	0.063	0.015	0.015	0.02
30393	121.564	316.665	326.861	-0.045	-0.077	0.015	0.015	0.015
30394	121.568	316.665	326.861	-0.045	0.063	0.015	0.015	0.015
30395	121.572	316.665	326.156	-0.045	-0.077	0.015	0.02	0.015
30396	121.576	317.368	326.156	-0.045	0.063	0.015	0.02	0.015
30397	121.58	316.665	326.861	-0.045	0.063	0.015	0.015	0.015
30398	121.584	317.368	326.861	-0.045	0.063	0.015	0.015	0.02
30399	121.588	317.368	326.156	-0.045	0.063	0.015	0.015	0.02
30400	121.592	318.07	326.156	-0.045	0.063	0.015	0.015	0.02
30401	121.596	318.07	326.861	-0.045	0.063	0.015	0.015	0.015

Appendix 7: Excerpt of the data from "Pure U-Tube with Water"

	A	B	C	D	E	F	G	H
15156	60.616	313.854	328.272	2.201	0.623	0.015	0.015	0.015
15157	60.62	311.746	328.272	2.201	0.483	0.015	0.015	0.015
15158	60.624	313.854	328.977	2.201	0.483	0.015	0.015	0.015
15159	60.628	313.151	328.272	2.201	0.483	0.015	0.015	0.015
15160	60.632	314.557	328.272	2.201	0.483	0.015	0.015	0.015
15161	60.636	313.151	328.272	2.201	0.483	0.015	0.015	0.02
15162	60.64	313.854	328.977	2.201	0.483	0.015	0.015	0.015
15163	60.644	313.854	328.272	2.201	0.483	0.015	0.015	0.015
15164	60.648	313.151	328.272	2.201	0.483	0.015	0.015	0.015
15165	60.652	315.259	328.272	2.342	0.623	0.015	0.015	0.015
15166	60.656	314.557	328.977	2.201	0.623	0.015	0.015	0.015
15167	60.66	314.557	328.272	2.201	0.483	0.015	0.015	0.015
15168	60.664	313.854	328.272	2.201	0.623	0.015	0.015	0.015
15169	60.668	312.448	328.272	2.201	0.623	0.015	0.015	0.015
15170	60.672	313.854	328.272	2.061	0.483	0.015	0.015	0.015
15171	60.676	313.151	328.272	2.201	0.483	0.015	0.015	0.015
15172	60.68	312.448	328.272	2.201	0.623	0.015	0.015	0.015
15173	60.684	313.151	328.272	2.201	0.483	0.015	0.015	0.015
15174	60.688	313.151	328.272	2.201	0.483	0.015	0.015	0.015
15175	60.692	313.854	328.272	2.201	0.623	0.02	0.015	0.015
15176	60.696	313.151	328.272	2.201	0.483	0.015	0.02	0.015
15177	60.7	315.259	328.272	2.201	0.623	0.015	0.015	0.015
15178	60.704	312.448	328.272	2.201	0.623	0.015	0.015	0.02
15179	60.708	313.854	328.272	2.201	0.483	0.015	0.015	0.015
15180	60.712	313.151	328.272	2.201	0.483	0.015	0.015	0.015
15181	60.716	313.854	328.272	2.201	0.483	0.015	0.015	0.024
15182	60.72	313.151	328.272	2.201	0.483	0.015	0.015	0.015
15183	60.724	313.151	328.272	2.201	0.623	0.015	0.015	0.015
15184	60.728	313.151	328.272	2.201	0.623	0.02	0.015	0.015
15185	60.732	313.151	328.272	2.201	0.483	0.015	0.02	0.015
15186	60.736	312.448	328.272	2.201	0.623	0.015	0.015	0.015
15187	60.74	313.854	328.977	2.342	0.623	0.015	0.015	0.02
15188	60.744	313.151	327.566	2.201	0.623	0.015	0.015	0.015
15189	60.748	313.854	328.272	2.201	0.623	0.015	0.015	0.015
15190	60.752	313.854	328.272	2.201	0.623	0.015	0.015	0.015
15191	60.756	313.151	328.977	2.342	0.623	0.015	0.015	0.015
15192	60.76	313.854	328.272	2.201	0.483	0.015	0.015	0
15193	60.764	313.854	328.272	2.201	0.483	0	0.015	0.015
15194	60.768	313.854	328.272	2.201	0.483	0.015	0.005	0.015
15195	60.772	314.557	328.272	2.201	0.623	0.015	0.015	0.015
15196	60.776	313.854	328.272	2.201	0.483	0.015	0.015	0.015
15197	60.78	314.557	328.272	2.342	0.764	0.015	0.015	0.015
15198	60.784	313.151	328.272	2.061	0.483	0.015	0.015	0.015
15199	60.788	313.854	328.272	2.201	0.483	0.015	0.015	0.015
15200	60.792	313.151	328.272	2.061	0.623	0.015	0.015	0.015
15201	60.796	312.448	328.272	2.201	0.483	0.015	0.02	0.02

Appendix 8: Excerpt of the data from "Pure U-Tube with 10g-l CMC"

	A	B	C	D	E	F	G	H
1151				Meas. Pt. Duration 5 s				
1152	Measuring Profile:							
1153	Shear Rate			d(gamma)/dt = 0,001 ... 1 000 1/s log; |Slope| = 6 Pt. / dec				
1154								
1155	Meas. Pts.	Shear Rate	Shear Stres	Viscosity	Speed	Torque	Status	Temperature
1156		[1/s]	[Pa]	[Pa·s]	[1/min]	[µNm]	[]	[°C]
1157	1	0.00037	-0.00136	-2.01	0.00016	-0.0641	Dy_auto	19.9857
1158	2	0.00147	-0.00184	-1.25	0.00024	-0.0601	Dy_auto	19.9886
1159	3	0.00215	-0.00175	-0.811	0.00035	-0.0571	Dy_auto	19.9894
1160	4	0.00316	-0.00168	-0.53	0.00052	-0.0549	Dy_auto	19.9868
1161	5	0.00464	-0.00146	-0.314	0.00076	-0.0477	Dy_auto	19.9881
1162	6	0.00681	-0.00124	-0.181	0.00112	-0.0404	Dy_auto	19.9896
1163	7	0.01	-0.0009	-0.0895	0.00164	-0.0293	Dy_auto	19.9883
1164	8	0.0147	-0.0003	-0.0203	0.00241	-0.00977	M- ,Dy_	19.9896
1165	9	0.0215	0.00031	0.0145	0.00354	0.0102	Dy_auto	19.9897
1166	10	0.0316	0.00081	0.0257	0.0052	0.0266	Dy_auto	19.9903
1167	11	0.0464	0.00166	0.0357	0.00763	0.0542	Dy_auto	19.99
1168	12	0.0681	0.00226	0.0332	0.0112	0.074	Dy_auto	19.992
1169	13	0.1	0.00304	0.0304	0.0164	0.0993	Dy_auto	19.9914
1170	14	0.147	0.004	0.0273	0.0241	0.131	Dy_auto	19.9927
1171	15	0.215	0.00468	0.0217	0.0354	0.153	Dy_auto	19.9918
1172	16	0.316	0.00606	0.0192	0.052	0.198	Dy_auto	19.9925
1173	17	0.464	0.00752	0.0162	0.0763	0.246	Dy_auto	19.9937
1174	18	0.681	0.0098	0.0144	0.112	0.321	Dy_auto	19.9943
1175	19	1	0.0125	0.0125	0.164	0.408	Dy_auto	19.9959
1176	20	1.47	0.0159	0.0108	0.241	0.519	Dy_auto	19.9948
1177	21	2.15	0.0191	0.00888	0.354	0.626	Dy_auto	19.9958
1178	22	3.16	0.0233	0.00737	0.52	0.763	Dy_auto	19.9962
1179	23	4.64	0.0323	0.00697	0.763	1.06	Dy_auto	19.9963
1180	24	6.81	0.045	0.00661	1.12	1.47	Dy_auto	19.997
1181	25	10	0.0662	0.00662	1.64	2.17	Dy_auto	19.9963
1182	26	14.7	0.0956	0.00651	2.41	3.13	Dy_auto	19.997
1183	27	21.5	0.139	0.00646	3.54	4.56	Dy_auto	19.9967
1184	28	31.6	0.198	0.00625	5.2	6.47	Dy_auto	19.9973
1185	29	46.4	0.289	0.00623	7.63	9.47	Dy_auto	19.9977
1186	30	68.1	0.419	0.00615	11.2	13.7	Dy_auto	19.999
1187	31	100	0.61	0.0061	16.4	20	Dy_auto	19.9972
1188	32	147	0.888	0.00605	24.1	29	Dy_auto	19.9972
1189	33	215	1.3	0.00602	35.4	42.4	Dy_auto	19.9989
1190	34	316	1.89	0.00598	52	61.9	Dy_auto	19.9976
1191	35	464	2.77	0.00596	76.3	90.6	Dy_auto	19.9986
1192	36	681	4.06	0.00595	112	133	Dy_auto	19.9968
1193	37	1 000	5.94	0.00594	164	194	Dy_auto	19.9981
1194								
1195	Interval:			2				
1196	Number of Data Points:			15				
1197								
1198	Time Setting:			19 Meas. Pts.				
1199				Meas. Pt. Duration 10 s				
1200	Measuring Profile:							
1201	Shear Rate			d(gamma)/dt = 1 020 ... 1 1/s log; |Slope| = 5,3828488 Pt. / de				
1202								
1203	Meas. Pts.	Shear Rate	Shear Stres	Viscosity	Speed	Torque	Status	Temperature
1204		[1/s]	[Pa]	[Pa·s]	[1/min]	[µNm]	[]	[°C]
1205	1	1 020	6.08	0.00596	168	199	Dy_auto	19.9973
1206	2	694	4.15	0.00598	114	136	Dy_auto	19.9973
1207	3	472	2.83	0.006	77.7	92.8	Dy_auto	19.9985
1208	4	321	1.94	0.00602	52.9	63.4	Dy_auto	19.998
1209	5	219	1.32	0.00605	36	43.3	Dy_auto	19.9991
1210	6	149	0.906	0.00608	24.5	29.6	Dy_auto	19.9994
1211	7	101	0.62	0.00612	16.7	20.3	Dy_auto	20.0011
1212	8	69	0.426	0.00617	11.3	13.9	Dy_auto	20
1213	9	46.9	0.292	0.00621	7.72	9.54	Dy_auto	20.0003
1214	10	31.9	0.2	0.00627	5.25	6.55	Dy_auto	19.9999
1215	11	21.7	0.139	0.0064	3.57	4.56	Dy_auto	19.9997
1216	12	14.8	0.095	0.00642	2.43	3.11	Dy_auto	19.9996
1217	13	10.1	0.0678	0.00673	1.66	2.22	Dy_auto	20.0006
1218	14	6.85	0.0474	0.00692	1.13	1.55	Dy_auto	20.0004
1219	15	4.66	0.0322	0.00691	0.767	1.05	Dy_auto	20.0003

Appendix 9: Excerpt of the data from "Rotational Shear Tests of CMC"

	A	B	C	D	E	F	G	H	I	J
822										
823	Meas. Pts.	Strain	Shear Stres	Storage M	Loss Modu	Damping F	Deflection	Torque	Status	Torque
824		[%]	[Pa]	[Pa]	[Pa]	[1]	[mrad]	[µNm]	[]	[mNm]
825	1	0.1	4.32E-05	1.19E-02	4.78E-02	4.02	0.0172	0.00161	M- ,DSO	1.6E-06
826	2	0.16	6.40E-05	7.37E-03	3.92E-02	5.32	0.0276	0.00203	DSO	2.1E-06
827	3	0.258	8.41E-05	3.26E-03	3.25E-02	9.95	0.0444	0.00275	DSO	2.8E-06
828	4	0.414	1.40E-04	0	3.40E-02	1 000 000	0.0712	0.0046	ME-,tsD	4.6E-06
829	5	0.664	2.12E-04	8.22E-04	3.20E-02	38.9	0.114	0.00695	DSO	7E-06
830	6	1.07	3.54E-04	0	3.32E-02	1 000 000	0.183	0.0116	ME-,tsD	1.2E-05
831	7	1.71	5.57E-04	9.18E-04	3.26E-02	35.5	0.294	0.0182	DSO	1.8E-05
832	8	2.74	8.95E-04	2.29E-03	3.25E-02	14.2	0.473	0.0293	DSO	2.9E-05
833	9	4.41	1.43E-03	2.73E-03	3.24E-02	11.9	0.759	0.0469	DSO	4.7E-05
834	10	7.07	2.31E-03	1.62E-03	3.26E-02	20.1	1.22	0.0755	DSO	7.6E-05
835	11	11.3	3.69E-03	3.81E-04	3.25E-02	85.3	1.95	0.121	DSO	0.00012
836	12	18.2	5.92E-03	0	3.25E-02	1 000 000	3.14	0.194	ME-,tsD	0.00019
837	13	29.2	9.52E-03	0	3.26E-02	1 000 000	5.04	0.312	ME-,tsD	0.00031
838	14	46.9	1.53E-02	0	3.26E-02	1 000 000	8.08	0.501	ME-,tsD	0.0005
839	15	75.3	2.46E-02	0	3.26E-02	1 000 000	13	0.805	ME-,tsD	0.00081
840	16	121	3.95E-02	0	3.27E-02	1 000 000	20.8	1.29	ME-,tsD	0.00129
841	17	194	6.29E-02	0	3.24E-02	1 000 000	33.4	2.06	ME-,tsD	0.00206
842	18	311	1.01E-01	0	3.23E-02	1 000 000	53.6	3.29	ME-,tsD	0.00329
843	19	500	1.61E-01	0	3.21E-02	1 000 000	86.1	5.25	ME-,tsD	0.00525
844										
845	Data Series Information									
846	Name:			CMC 100g/l 7rad/sec 1						
847	Number of Intervals:			1						
848	Application:			RHEOPLUS/32 V3.62 21006454-33024						
849	Device:			MCR302 SN81193523; F'W3.67; Slot(3,-1); Adj(139,0)d						
850	Measuring Date/Time:			27.05.2013; 18:50						
851	Measuring System:			CP50-1-SN30011; d=0,036 mm						
852	Accessories:			TU1=P-PTD200-SN81221738						
853										
854	Calculating Constants:									
855	- Cor [min/s]:			6.08127						
856	- Css [Pa/mNm]:			30.5568						
857	- Start Delay Time [s]:			7.993						
858	- Substance Density [rho]:			1000						
859	- Measurement Type:			0						
860	- Axial Compliance [m/N]:			1.00E-06						
861	- Position [m]:			1.00E-06						
862										
863	Interval:			1						
864	Number of Data Points:			19						
865										
866	Time Setting:			19 Meas. Pts.						
867	Measuring Profile:									
868	#NAME?			Amplitude gamma = 0,1 ... 500 % log; |Slope| = 4,8662195 Pt. / dec						
869				Angular Frequency omega = 7 rad/s						
870										
871	Meas. Pts.	Strain	Shear Stres	Storage M	Loss Modu	Damping F	Deflection	Torque	Status	Torque
872		[%]	[Pa]	[Pa]	[Pa]	[1]	[mrad]	[µNm]	[]	[mNm]
873	1	0.1	4.13E-05	0	4.13E-02	1 000 000	0.0172	0.00135	M- ,ME-	1.4E-06
874	2	0.161	7.29E-05	0	4.54E-02	1 000 000	0.0276	0.00239	ME-,tsD	2.4E-06
875	3	0.258	1.17E-04	0	4.56E-02	1 000 000	0.0444	0.00385	ME-,tsD	3.9E-06
876	4	0.413	1.83E-04	0	4.43E-02	1 000 000	0.0712	0.006	ME-,tsD	6E-06
877	5	0.664	3.02E-04	0	4.56E-02	1 000 000	0.114	0.0039	ME-,tsD	3.9E-06
878	6	1.07	4.32E-04	0	4.62E-02	1 000 000	0.183	0.0161	ME-,tsD	1.6E-05
879	7	1.71	7.84E-04	0	4.59E-02	1 000 000	0.294	0.0257	ME-,tsD	2.6E-05
880	8	2.74	1.24E-03	0	4.53E-02	1 000 000	0.473	0.0407	ME-,tsD	4.1E-05
881	9	4.41	1.99E-03	0	4.51E-02	1 000 000	0.759	0.0651	ME-,tsD	6.5E-05
882	10	7.07	3.19E-03	5.56E-04	4.52E-02	81.2	1.22	0.104	DSO	0.0001
883	11	11.3	5.13E-03	1.74E-03	4.52E-02	26	1.95	0.168	DSO	0.00017
884	12	18.2	8.24E-03	5.70E-04	4.52E-02	79.4	3.14	0.27	DSO	0.00027
885	13	29.2	1.32E-02	9.37E-04	4.52E-02	45.3	5.04	0.433	DSO	0.00043
886	14	46.9	2.13E-02	9.20E-04	4.53E-02	49.3	8.08	0.696	DSO	0.0007
887	15	75.3	3.37E-02	2.52E-04	4.48E-02	178	13	1.1	DSO	0.0011
888	16	121	5.42E-02	1.77E-04	4.48E-02	254	20.8	1.77	DSO	0.00177
889	17	194	8.69E-02	0	4.48E-02	1 000 000	33.4	2.84	ME-,tsD	0.00284
890	18	312	1.39E-01	0	4.46E-02	1 000 000	53.6	4.55	ME-,tsD	0.00455
891	19	500	2.22E-01	0	4.44E-02	1 000 000	86.1	7.27	ME-,tsD	0.00727

Appendix 10: Excerpt of the data from "Amplitude Sweep Oscillation Tests of CMC"